

1 **Thorium isotopes tracing the iron cycle at the Hawaii Ocean Time-series Station ALOHA**

2 Christopher T. Hayes<sup>a,\*</sup>, Jessica N. Fitzsimmons<sup>a,1</sup>, Edward A. Boyle<sup>a</sup>, David McGee<sup>a</sup>, Robert F.  
3 Anderson<sup>b</sup>, Rachel Weisend<sup>c</sup> and Peter L. Morton<sup>c</sup>

4 <sup>a</sup>Department of Earth, Atmospheric and Planetary Sciences, Massachusetts Institute of  
5 Technology, Cambridge, MA

6 <sup>b</sup>Lamont-Doherty Earth Observatory of Columbia University, Palisades, NY

7 <sup>c</sup>Department of Earth, Ocean, and Atmospheric Science, Florida State University, Tallahassee FL

8 <sup>1</sup>Now at Department of Oceanography, Texas A&M University, College Station, TX

9 \*Corresponding author: cthayes@mit.edu

10 **Abstract**

11 The role of iron as a limiting micronutrient motivates an effort to understand the supply and  
12 removal of lithogenic trace metals in the ocean. The long-lived thorium isotopes (<sup>232</sup>Th and  
13 <sup>230</sup>Th) in seawater can be used to quantify the input of lithogenic metals attributable to the partial  
14 dissolution of aerosol dust. Thus, Th can help in disentangling the Fe cycle by providing an  
15 estimate of its ultimate supply and turnover rate. Here we present time-series (1994-2014) data  
16 on thorium isotopes and iron concentrations in seawater from the Hawaii Ocean Time-series  
17 Station ALOHA. By comparing Th-based dissolved Fe fluxes with measured dissolved Fe  
18 inventories, we derive Fe residence times of 6-12 months for the surface ocean. Therefore, Fe  
19 inventories in the surface ocean are sensitive to seasonal changes in dust input. Ultrafiltration  
20 results further reveal that Th has a much lower colloidal content than Fe does, despite a common  
21 source. On this basis, we suggest Fe colloids may be predominantly organic in composition, at  
22 least at Station ALOHA. In the deep ocean (>2 km), Fe approaches a solubility limit while Th,  
23 surprisingly, is continually leached from lithogenic particles. This distinction has implications  
24 for the relevance of Fe ligand availability in the deep ocean, but also suggests Th is not a good  
25 tracer for Fe in deep waters. While uncovering divergent behavior of these elements in the water  
26 column, this study finds that dissolved Th flux is a suitable proxy for the supply of Fe from dust  
27 in the remote surface ocean.

## 28 **1. Introduction**

29           Determination of the supplies of iron to the ocean is relevant to understanding Earth's  
30 climate and the ocean's ecology. Ocean storage of carbon dioxide is mediated by iron supply in  
31 large areas of the ocean where Fe is a limiting resource, both today (Moore et al., 2013) and  
32 during the ice ages (Martínez-García et al., 2014). Additionally, the marine distribution of  
33 diazotrophic phytoplankton that modulate the nitrogen cycle may be determined by Fe supply  
34 rates (Ward et al., 2013). Atmospheric dust is arguably the major source of Fe to the euphotic  
35 zone (Boyd et al., 2010; Conway and John, 2014; Jickells et al., 2005; Tagliabue et al., 2014).  
36 Debate on the sources of marine Fe ensues largely because the techniques to estimate the supply  
37 rate of Fe from dust in particular, or Fe residence times in general, are only beginning to be  
38 developed.

39           In this study, we assess the utility of thorium isotopes in seawater to provide rate  
40 information on the Fe cycle. By pairing  $^{232}\text{Th}$ , sourced from dust, with radiogenic  $^{230}\text{Th}$  (or  
41  $^{234}\text{Th}$ ) that provides a timescale of thorium flux, one can make quantitative estimates of both the  
42 total dust flux to the ocean (Deng et al., 2014; Hsieh et al., 2011) and the flux of trace metals  
43 released by dust dissolution (Hayes et al., 2013a). Our study site is the Hawaii Ocean Time-  
44 series Station ALOHA ( $22^\circ 45' \text{ N}$ ,  $158^\circ \text{ W}$ ) (Church et al., 2013; Karl and Lukas, 1996) in the  
45 subtropical North Pacific, where Asian dust is deposited in spring (Boyle et al., 2005; Hyslop et  
46 al., 2013; Prospero et al., 2003). Presenting time-series data spanning 20 yrs (1994-2014), we  
47 demonstrate that the behaviors of Fe and Th in seawater are consistent with a variable dust  
48 source to the surface ocean. Thorium-based fluxes indicate that the residence time of dissolved  
49 Fe in the upper 125 m of the water column is less than one year. In the sub-surface ocean ( $>250$

50 m), the thorium and iron cycles begin to diverge considerably. These divergences reveal new  
51 insights into the marine geochemistry of these elements.

## 52 **2. Background**

### 53 *2.1 Finding the timescale: thorium removal*

54 The rate information on trace metal cycling that we seek is obtained by exploiting the  
55 natural radioactive disequilibrium between insoluble  $^{230}\text{Th}$  and its soluble parent  $^{234}\text{U}$  in  
56 seawater. The oceanic distribution of  $^{234}\text{U}$  (half-life 245,620 yrs (Cheng et al., 2013)) is  
57 homogeneous within a few parts per thousand, as  $^{238}\text{U}$  concentrations vary only with salinity  
58 (Owens et al., 2011) and  $^{234}\text{U}/^{238}\text{U}$  ratios vary by less than 1 per mil (Andersen et al., 2010).  
59 Therefore, the decay of  $^{234}\text{U}$  produces  $^{230}\text{Th}$  at a known rate everywhere in the ocean. Due to its  
60 particle reactivity, thorium adsorbs onto sinking particulate matter, a process called scavenging,  
61 on a timescale of years to decades, much faster than  $^{230}\text{Th}$  decay (half-life 75,584 yrs (Cheng et  
62 al., 2013)).

63 Thus by comparing the amount of  $^{230}\text{Th}$  that remains in seawater to the amount produced  
64 by U decay, one can calculate a removal timescale (Eq. 1, Fig. 1), or residence time ( $\tau$ ), of  
65 thorium in seawater. Equation 1 is written with radionuclide concentrations in terms of activity  
66 (decays per unit time per unit seawater). The denominator contains a  $^{230}\text{Th}$  term to account for  
67  $^{230}\text{Th}$ -decay, which, as mentioned above, can be neglected on the timescale of water column  
68 processes (for instance, seawater  $^{234}\text{U}$  activity is 46.6 mBq/kg at salinity 35, while typical  $^{230}\text{Th}$   
69 activities are 1-10  $\mu\text{Bq/kg}$ ). This approach is analogous to that used with a more commonly used  
70 flux tracer, the shorter-lived  $^{234}\text{Th}$  (half-life 24.1 days). By the same principles, using its  
71 production rate from parent isotope  $^{238}\text{U}$ ,  $^{234}\text{Th}$  inventories can also be used to determine the  
72 scavenging rate of Th in seawater (Buesseler et al., 1992; Coale and Bruland, 1985), except that

73  $^{234}\text{Th}$ -decay is much more significant in the water column balance ( $^{238}\text{U}$  activities being ~40  
74 mBq/kg compared to euphotic zone  $^{234}\text{Th}$  activities of 30-40 mBq/kg).

$$75 \quad \tau_{Th}(z) = \frac{\int_0^z {}^{230}\text{Th} dz}{\int_0^z ({}^{234}\text{U} - {}^{230}\text{Th}) * \lambda_{230} dz} \quad \text{Eq. 1}$$

76 To meet the requirements of a steady-state assumption between source and removal  
77 terms, we calculate thorium residence times in an integrated sense, from the surface to a  
78 particular depth. Thus as one integrates deeper into the water column, the  $^{230}\text{Th}$  inventories  
79 reflect longer timescales of removal. Residence times calculated in this way also neglect  
80 dispersal fluxes by ocean circulation. Lateral gradients in oceanic  $^{230}\text{Th}$  concentrations are  
81 generally small (Hayes et al., 2015a), while large vertical gradients may make vertical fluxes  
82 significant, for instance due to upwelling (Luo et al., 1995).

### 83 *2.2 Finding the source: lithogenic metal fluxes*

84 The dominant isotope of seawater thorium is primordial and long-lived (half-life 14.1 x  
85  $10^9$  yrs)  $^{232}\text{Th}$ . It is added to the ocean only through the partial dissolution of continental  
86 material, which in the context of Station ALOHA we consider to be primarily aerosol dust. Once  
87 in the water column,  $^{232}\text{Th}$  is assumed to undergo scavenging removal (Fig. 1) at the same rate,  
88 i.e. with the same residence time, as  $^{230}\text{Th}$  (or  $^{234}\text{Th}$ ), as scavenging tendencies are characteristic  
89 of all isotopes of an element. Assuming a steady state for Th concentrations, with knowledge of  
90 the Th residence time derived from  $^{230}\text{Th}$ , one can calculate the flux of dust-derived  $^{232}\text{Th}$   
91 necessary to support the observed  $^{232}\text{Th}$  inventory (Eq. 2). As in calculating thorium residence  
92 times, the derived dissolved  $^{232}\text{Th}$  flux is reflective of the integrated depth zone, rather than at a  
93 particular depth. More details on  $^{232}\text{Th}$  flux calculations are reported by Hayes et al. (2013a).

$$94 \quad {}^{232}\text{Th flux}(z) = \frac{\int_0^z {}^{232}\text{Th} dz}{\tau_{Th}(z)} \quad \text{Eq. 2}$$

95 In comparison to the relative simplicity of the supply and removal terms in the thorium  
 96 cycle, seawater iron cycling has many more terms to consider. These include biological uptake,  
 97 remineralization, redox chemistry, anthropogenic or hydrothermal sources, in addition to supply  
 98 by dust and removal by scavenging (Fig. 1). Scavenging of Fe also occurs but at a different rate  
 99 than that of Th. The utility of this element pair is their common source from dust. This is, of  
 100 course, an idealization of the “simple” thorium cycle. Th will be involved to some extent with  
 101 (perhaps inadvertent) uptake into and remineralization from organic matter (Barbeau et al., 2001;  
 102 Hirose and Tanoue, 1994). We have also observed a strong hydrothermal sink for Th in the  
 103 Atlantic (Hayes et al., 2015a) in addition to an abyssal source of Th from sediments in the North  
 104 Pacific (Hayes et al., 2013a). Nonetheless, particularly in the remote surface ocean well above  
 105 the seafloor, dust dissolution and scavenging appear to be the dominant terms for Th cycling.  
 106 Thus, in this manuscript we propose using dissolved  $^{232}\text{Th}$  flux as a proxy for the Fe released  
 107 during dust dissolution. This can be done with knowledge of the Fe/Th ratio in the dust and the  
 108 relative fractional solubility of the two elements ( $S_{\text{Fe/Th}}$ , Eq. 3).

$$109 \quad \text{Dust-dissolved Fe flux} = \text{dissolved } ^{232}\text{Th flux} \times (\text{Fe/Th})_{\text{dust}} \times S_{\text{Fe/Th}} \quad \text{Eq. 3}$$

110 By weight, the Asian desert dust that undergoes long-range transport over the North  
 111 Pacific contains  $^{232}\text{Th}$  at  $14.3 \pm 0.8$  ppm, based on fine grained ( $<8 \mu\text{m}$ ) source materials  
 112 (McGee, 2009; Serno et al., 2014), and Fe at  $3.8 \pm 0.4$  %, based on a literature compilation by  
 113 Mahowald et al. (2005). Therefore, we assume the Fe/Th ratio in dust at Station ALOHA of  $2660$   
 114  $\pm 320$  g/g or  $11,040 \pm 1450$  mol/mol. These ratios are close to the average for the upper  
 115 continental crust of  $\text{Fe/Th} = 3271$  g/g =  $13,553$  mol/mol (Taylor and McLennan, 1995).

116 The relative fractional solubility of Fe and Th in dust is currently unconstrained. Hayes et  
 117 al. (2013a) assumed  $S_{\text{Fe/Th}} = 1$  as a starting point, based solely on the similarly insoluble nature

118 of these two elements in seawater. While much more work is needed to constrain this parameter,  
119 here we continue to assume  $S_{\text{Fe/Th}} = 1$ , and our observations of the time-series variability in the  
120 seawater  $\text{Fe}/^{232}\text{Th}$  ratio (section 4.4) support this assumption.

### 121 *2.3 Iron residence times*

122 We cannot rule out significant marine Fe sources by anthropogenic (e.g., derived from  
123 fossil fuel combustion) aerosols, continental margin sediments, or deep-sea hydrothermal vents.  
124 We can, however, pursue the notion that if dust were the only Fe source to the water column, the  
125 comparison between measured dissolved Fe inventories to the source (dust-dissolved Fe flux)  
126 would produce a measure of the turnover rate or residence time of dissolved Fe in seawater (Eq.  
127 4). This residence time again represents the residence time within the integrated water column.  
128 Additional sources of Fe, such as combustion aerosols or hydrothermal fluids, would cause the  
129 dust-based Fe residence time to be an overestimate. Relevant to iron cycling, this residence time  
130 provides a rough timescale over which one can expect Fe concentration to vary as a result of  
131 variation in sources, such as springtime Asian dust events (Boyle et al., 2005).

$$132 \quad \text{Dissolved Fe residence time} = \text{Fe inventory} \div \text{dust-dissolved Fe flux} \quad \text{Eq. 4}$$

## 133 **3. Materials and Methods**

134

### 135 *3.1 Sample collection during 2012-2014*

136

137 Samples were collected on several cruises on the R/V *Kilo Moana*, led by the Center for  
138 Microbial Oceanography: Research and Education (C-MORE), to Station ALOHA in July-  
139 September 2012 (HOE-DYLAN), May-June 2013 (HOE-PhoR-I), September 2013 (HOE-PhoR-  
140 II) and March 2014 (HOE-BOE-I). Depth profiles for  $^{230}\text{Th}/^{232}\text{Th}$  analysis were collected from

141 the ship's Niskin bottle rosette, filtered with a 0.45  $\mu\text{m}$  Acropak cartridge filter, and acidified to  
142 pH 1.8 with Savillex-distilled 6 M HCl.

143 Filtered surface seawater (0.4  $\mu\text{m}$ ) was collected for  $^{232}\text{Th}$  (which requires smaller  
144 volumes than for  $^{230}\text{Th}$ ), as well as for dissolved Fe, using the trace-metal clean MITESS  
145 sampler (Bell et al., 2002) at near daily time intervals on the 2012-2013 C-MORE cruises.  
146 MITESS collection methods, including "Vane" sampling for Fe depth profiles, on the HOE  
147 campaigns are discussed fully by Fitzsimmons et al. (in review). Within 3 hours of collection, the  
148 seawater was filtered using 0.4  $\mu\text{m}$  polycarbonate track etch filters (PCTE, Whatman).  
149 Particulate samples were immediately frozen, and dissolved filtrates were acidified to pH 2 with  
150 trace metal clean HCl. The filters used for filtering MITESS water were analyzed for particulate  
151 Fe and  $^{232}\text{Th}$  (representing on average 0.7 liters of seawater).

152 On HOE-PhoR-II, cross flow filtration was performed to assess colloidal  $^{232}\text{Th}/^{230}\text{Th}$   
153 using protocols developed to study colloidal Fe (Fitzsimmons and Boyle, 2014a). Seawater was  
154 pre-filtered at 0.45  $\mu\text{m}$  and, within 1-2 hours, pumped over a Millipore Pellicon XL filter made  
155 of regenerated cellulose with a nominal molecular weight cutoff of 10 kDa, roughly equivalent to  
156 an effective pore size of 10 nanometers. Both permeate and retentate fractions were analyzed to  
157 determine any loss of Th by adsorption, which turned out to be minimal (88-100% dissolved Th  
158 recovery).

### 159 *3.2 Hawaii Ocean Time-series (HOT) seawater*

160 Seawater samples, typically 0.5 liter size, have been collected during the HOT program  
161 for trace metal analysis at MIT periodically since 1997. Most of these samples were collected as  
162 unfiltered water using the MITESS sampler (Bell et al., 2002) and subsequently preserved by  
163 acidification to pH 2 with HCl. We report data from samples collected via ship-based MITESS

164 collections as well as MITESS units deployed on a mooring (1997-2000, 2004-2005). In ship-  
165 board sampling, a sample bottle filled with high-purity dilute (~0.001 M) HCl is lowered over  
166 the side on a clean-wire and opened at depth, allowing ~15-20 minutes for the bottle to be  
167 completely flushed with the denser seawater, before bottle closure and sample retrieval. The  
168 moored sampling worked similarly except that bottles were filled with stronger acid (1 M HCl)  
169 prior to sampling. The moored sampling potentially posed a metal contamination risk due to the  
170 effective stronger leaching of the HDPE bottles, increasing the chance for leached Th, for  
171 example, to remain in the sample bottle at the time of collection. We report the moored sampler  
172 data with a unique symbol in our figures and interpret them with caution. Further sampling  
173 details are given by Boyle et al. (2005).

174 We also make use of literature seawater  $^{232}\text{Th}/^{230}\text{Th}$  data, collected at Station ALOHA in  
175 September 1994 (HOT-57), reported by Roy-Barman et al. (1996).

### 176 *3.3 Thorium and iron analyses*

177 Dissolved  $^{230}\text{Th}$  concentrations at Station ALOHA are as low as  $10^{-18}$  moles per kilogram  
178 seawater ( $10^{-18} \text{ mol } ^{230}\text{Th} = 0.1746 \text{ } \mu\text{Bq}$ ). Therefore, for measurement by inductively-coupled  
179 plasma mass spectrometry (ICP-MS), 4-5 liter water samples are required. Thorium  
180 concentrations were determined by isotope dilution by spiking with  $^{229}\text{Th}$  (not present in natural  
181 seawater). Sample preparation (pre-concentration, acid digestion, and chromatographic  
182 purification) was performed using published methods (Anderson et al., 2012; Auro et al., 2012).  
183 A portion of the  $^{230}\text{Th}$  samples were prepared and analyzed at the Lamont-Doherty Earth  
184 Observatory (L-DEO), using an Element XR single-collector ICP-MS. The remaining  $^{230}\text{Th}$   
185 samples were prepared at the Massachusetts Institute of Technology (MIT) and analyzed using a



186 Neptune Plus multi-collector ICP-MS at Brown University. Th-232 was also analyzed in samples  
187 prepared for  $^{230}\text{Th}$ .

188 Analysis of  $^{232}\text{Th}$ , at  $10^{-15}$  mol (i.e. femtomoles) per kg seawater, required smaller  
189 samples (200-800 mL) and was measured on archive HOT and HOE samples for which sample  
190 volume did not allow  $^{230}\text{Th}$  determination. While not as prone to contamination as some other  
191 trace elements, clean lab techniques were required to produce blanks that were consistent and  
192 low enough to allow detection of the relatively small sample size of ~20-40 femtomoles  $^{232}\text{Th}$ .  
193 Therefore, modifications of the cited procedures for Th analysis (Anderson et al., 2012; Auro et  
194 al., 2012) were made. Instead of co-precipitation with added Fe, pre-concentration of  $^{232}\text{Th}$  was  
195 achieved using magnesium hydroxide co-precipitation, such as that described for Pb by Reuer et  
196 al. (2003). Thorium was purified using a smaller amount (100  $\mu\text{l}$  rather than 1 ml) of anion-  
197 exchange resin (AG1-X8) on columns fashioned from Teflon shrink-tubing. Samples were  
198 loaded onto AG1-X8 resin in 8 M  $\text{HNO}_3$  and Th was eluted with 6 M HCl (instead of 12 M HCl,  
199 to reduce acid blank), following Edwards et al. (1987). Blank determinations were made on 125  
200 mL aliquots of acidified seawater samples whose  $^{232}\text{Th}$  content had been determined during  
201 previous  $^{230}\text{Th}$  analysis. The mean procedural blank ( $n = 6$ ) was  $3.5 \pm 1.6$  fmol  $^{232}\text{Th}$ , resulting in  
202 a detection limit of 4.8 fmol  $^{232}\text{Th}$ . Samples for seawater  $^{232}\text{Th}$  were prepared and analyzed at  
203 MIT, using a Micromass IsoProbe multi-collector ICP-MS with detection by a Daly-style ion  
204 counter.

205 In this study, we refer to measured trace metal concentrations as dissolved (filtered at 0.4  
206 or 0.45  $\mu\text{m}$ ), particulate ( $>0.4$   $\mu\text{m}$ ), or total (acidified unfiltered water). The “total”  
207 concentrations in this sense are sometimes referred to as “total dissolvable”, allowing for the  
208 possibility that some forms of Th are not mobilized into solution by acidification to pH 2 or

209 collected with co-precipitation. Since our goal in interpreting seawater  $^{230}\text{Th}$  concentrations is to  
210 determine scavenging rates based on uranium decay, we made small (0-10%) corrections for the  
211 dissolved  $^{230}\text{Th}$  released from dust (or lithogenic material in general). This correction is based on  
212 measured dissolved  $^{232}\text{Th}$  and a lithogenic  $^{230}\text{Th}/^{232}\text{Th}$  mole ratio of  $4 \times 10^{-6}$  (Roy-Barman et al.,  
213 2009). The corrected dissolved  $^{230}\text{Th}$  values are denoted as “xs”.

214 Particulate  $^{232}\text{Th}$  and particulate Fe, were analyzed at Florida State University by total  
215 digestion of the filter samples and subsequent analysis by ICP-MS, using slightly modified  
216 versions of published protocols (Ho et al., 2011; Morton et al., 2013; Upadhyay et al., 2009). In  
217 brief, samples were microwaved (CEM MARS Xpress) for 40 minutes at  $180^\circ\text{C}$  with  $\text{HNO}_3$  and  
218  $\text{H}_2\text{O}_2$  (to digest the organic and less refractory biogenic and authigenic components) and HF (to  
219 digest the more refractory lithogenic components). The detection limit (based on 3 standard  
220 deviations of the digested acid blanks) for particulate  $^{232}\text{Th}$  was 8 fmol/L (n=19) and the  
221 particulate Fe detection limit was 0.2 nmol/L (n=21). Dissolved Fe was measured by isotope  
222 dilution after pre-concentration onto nitrilotriacetate resin on the Micromass IsoProbe ICP-MS at  
223 MIT (Lee et al., 2011). Further details on Fe analyses are discussed by Fitzsimmons et al. (in  
224 review).

225 Data presented in this study can be accessed in the Supplemental Material online.

## 226 **4. Results and Discussion**

227

### 228 *4.1 $^{230}\text{Th}$ - $^{232}\text{Th}$ depth profiles to 1.5 km*

229

230 We focus first on the 2012-2013 thorium isotope depth profiles in the upper 1.5 km of the  
231 water column for a sense of the type of data used to calculate thorium fluxes (Fig. 2). High  
232 resolution depth profiles were analyzed in late July 2012, early June 2013 and late September  
233 2013. The mixed layer depths during these sampling casts (based on  $0.125 \text{ kg/m}^3$  density change)

234 were 54, 33 and 53 m, respectively, and below 100 m these profiles displayed little  
235 distinguishing hydrography (Figs. 2C, 2D, 2E).

236 For dissolved  $^{232}\text{Th}$  (Fig. 2A), there were increased concentrations near the surface,  
237 minimum concentrations at the depth of maximum chlorophyll concentration (the DCM, ~120-  
238 140 m), and a relatively constant local concentration maximum at 500-600 m depth. At  
239 intermediate depths (900-1200 m), each profile exhibited smooth variations in concentration but  
240 concentrations at the different sampling dates varied by up to 30%.

241 The surface  $^{232}\text{Th}$  maxima are consistent with aerosol dust as the major source of  $^{232}\text{Th}$  to  
242 Station ALOHA, as recognized by Roy-Barman et al. (1996). An interesting feature of these  
243 high-depth resolution measurements is that the surface (5 m)  $^{232}\text{Th}$  concentration was lower than  
244 that in the core of the mixed layer (25 m depth) at these three sampling times. This is perhaps  
245 related to small-scale scavenging and export dynamics, or particle cycling in general.

246 The coincidence of the subsurface chlorophyll maximum and the minimum in  $^{232}\text{Th}$  is  
247 apparently a universal feature for lithogenic trace elements such as Al, Ti and Fe (Dammshäuser  
248 et al., 2013; Fitzsimmons and Boyle, 2014b; Ohnemus and Lam, 2015). This was also true for  
249 dissolved and particulate Fe at Station ALOHA during this study (Fitzsimmons et al., in review).  
250 Increased particle aggregation efficiency, such as through the formation of fecal pellets, may  
251 more efficiently scavenge dissolved  $^{232}\text{Th}$  from this depth.

252 Scavenged  $^{232}\text{Th}$  may be partially released through remineralization of particles from the  
253 near-surface upon sinking to mesopelagic depths (300-500 m). Thus remineralization may be  
254 responsible for some of the subsurface  $^{232}\text{Th}$  maxima at 400-600 m depth. In support of this  
255 view, this depth range coincides with a rapid increase in phosphate concentration and apparent  
256 oxygen utilization, as inferred from HOT climatology

257 (<http://hahana.soest.hawaii.edu/hot/trends/trends.html>). On the other hand, the attenuation of  
258 particulate organic carbon at Station ALOHA is most intense at shallower depths, between 100  
259 and 200 m (Bishop and Wood, 2008).

260 The dominant basalts of the Hawaiian Islands (tholeiitic) are low in Th content,  $0.8 \pm 0.4$   
261 ppm, according to available data in PetDB ([www.earthchem.org/petdb](http://www.earthchem.org/petdb)) (Lehnert et al., 2000).  
262 Nonetheless, with our seawater observations, we cannot fully rule out lateral input of Th from  
263 the Hawaiian Islands. For instance, dissolved Mn concentrations reach a maximum near 800 m  
264 depth at Station ALOHA (Boyle et al., 2005) that may reflect a coastal source of metals.

265 The variability in  $^{232}\text{Th}$  concentration at intermediate depths (900-1400 m) could be due  
266 to the effect of hydrothermal activity at the nearby Loihi seamount. The iron oxide particles  
267 associated with hydrothermal plumes strongly scavenge Th, and depleted deep-sea Th  
268 concentrations have been observed up to 1400 km away from a vent site in the Atlantic (Hayes et  
269 al., 2015a). While intermediate water  $^{232}\text{Th}$  variability suggests the influence of hydrothermal  
270 scavenging here, the effect is apparently too weak to perturb the near-linear  $^{230}\text{Th}$  profiles (Fig.  
271 2). Time-variability in the influence of the Loihi hydrothermal system on trace metals at  
272 ALOHA is discussed more fully by Fitzsimmons et al. (in review).

273 The  $^{230}\text{Th}$  profiles also displayed interesting temporal variations. The theory of reversible  
274 scavenging contends that a steady-state is achieved between thorium adsorption and desorption  
275 on uniform particles that settle at a constant rate (Bacon and Anderson, 1982). Under these  
276 assumptions, one expects  $^{230}\text{Th}$  concentrations to increase linearly with depth with a boundary  
277 condition of zero concentration at the surface. While the observed depth profiles are essentially  
278 linear (Fig. 2B), it appears that mixing at the surface homogenizes  $^{230}\text{Th}$  concentrations to some  
279 depth. Interestingly, the layer of relatively homogeneous  $^{230}\text{Th}$  extends deeper than the density-

280 defined mixed layer (30-50 m), down to the deep chlorophyll maximum (Fig. 2; see also report  
281 by Barone et al. (2015)). This phenomenon is worthy of future time-series study. Potentially a  
282 remnant of deep winter mixed layers (> 100 m), the homogeneous surface  $^{230}\text{Th}$  layer could also  
283 represent some combination of vertical mixing and enhanced scavenging related to export of  
284 organic matter from the euphotic zone.

285 Another significant observation is that while the surface  $^{230}\text{Th}$  concentrations from June  
286 and September 2013 were nearly identical (1.2  $\mu\text{Bq/kg}$ ), the surface  $^{230}\text{Th}$  concentrations from  
287 July 2012 were about a factor of 2 lower (0.6  $\mu\text{Bq/kg}$ ). This implies a relatively rapid change in  
288 scavenging and/or export production. Future time-series studies are warranted to further assess  
289 the short-term (daily-monthly) variability in euphotic zone  $^{230}\text{Th}$  concentrations and how closely  
290 these changes can be correlated with organic matter export. In the next section, we assess what  
291 changes in the removal timescale are implied by these results.

#### 292 *4.2 Surface thorium residence times*

293  
294 Residence times of dissolved  $^{230}\text{Th}$  as described in section 2.1 using the 2012-2014  
295 results are presented in Figure 3. In this assessment, we integrate production due to  $^{234}\text{U}$  decay  
296 (based on salinity) and the measured  $^{230}\text{Th}$  inventory to 150 m depth. This allows comparison to  
297 Th residence times calculated on the basis of  $^{234}\text{Th}$ : $^{238}\text{U}$  disequilibrium established by previous  
298 work at Station ALOHA, during April 1999-March 2000 (Benitez-Nelson et al., 2001) and June-  
299 July 2008 (Buesseler et al., 2009). The  $^{234}\text{Th}$  results differ slightly from the approach used here  
300 for dissolved  $^{230}\text{Th}$  since the  $^{234}\text{Th}$  fluxes are calculated using unfiltered seawater. Since  
301 adsorbed  $^{230}\text{Th}$  concentrations are on the order of ~10-20% of total  $^{230}\text{Th}$  (Roy-Barman et al.,  
302 1996), residence times based on total  $^{234}\text{Th}$  can be expected to be up to 10-20% greater than  
303 those based on the dissolved phase only. The low percentage of adsorbed  $^{230}\text{Th}$  appears to hold

304 generally for the remote ocean (Hayes et al., 2015b), but it could be higher in coastal or marginal  
305 seas with high terrigenous or riverine input (e.g., (Andersson et al., 1995)).

306 We also assessed the influence of vertical mixing on surface  $^{230}\text{Th}$  inventories, which  
307 could influence the derived residence time. Assuming a vertical mixing coefficient ( $K_v$ ) of  $10^{-5}$   
308  $\text{m}^2/\text{s}$  (Charette et al., 2013), using a linear regression of the  $^{230}\text{Th}$  depth profiles (from 150 to 300  
309 m), we can calculate the  $^{230}\text{Th}$  added to the upper 150 m by vertical mixing as  $K_v \times d\text{Th}/dz$ . The  
310 results indicate that this vertical mixing term is 3-5% of the integrated production due to  $^{234}\text{U}$   
311 decay in the upper 150 m. Therefore we can assume that vertical mixing does not significantly  
312 affect the  $^{230}\text{Th}$  residence time estimates at Station ALOHA.

313 Nearly all of the thorium residence time estimates fall in the range of 1 to 3 years with no  
314 evident seasonal cycle (Fig. 3). In the HOT climatology, organic carbon export at 150 m is  
315 highest in May-August. While export seasonality is relatively weak in this oligotrophic,  
316 subtropical location (Church et al., 2013), long-term monitoring has revealed episodic export  
317 events related to diatom blooms and symbiotic cyanobacteria, typically in late July and early  
318 August (Karl et al., 2012).

319 The concept of “residence time” used here is based on a steady-state assumption for  
320 sources and sinks. Therefore with a residence time of  $\sim 2$  years, one would not expect significant  
321 variation in the removal timescale over a period of months. However, the range in observed Th  
322 residence times for Station ALOHA indicates that this steady-state assumption is not quite  
323 correct. More precisely, the steady-state for scavenging removal of Th appears to hold within a  
324 factor of 2-3. The range in removal timescales observed based on  $^{230}\text{Th}$  is similar to that based on  
325  $^{234}\text{Th}$ . Thus, it seems the rate of thorium scavenging can change dynamically at Station ALOHA

326 possibly related to export pulses, but the data are consistent with a long-term average thorium  
327 residence time of  $2 \pm 1$  years in the upper 150 m.

#### 328 *4.3 Surface $^{232}\text{Th}$ concentrations*

329 With relatively good control on the removal timescale of thorium, we turn to observed  
330 variability in surface  $^{232}\text{Th}$  concentrations. Barring significant fluxes due to lateral circulation,  
331 this variability represents the balance between removal by scavenging and input by dust. Smaller  
332 volume requirements for analysis (<1 liter) allowed us to investigate  $^{232}\text{Th}$  from daily, monthly  
333 and decadal timescales.

334 Collected during a series of cruises in summer 2012 (HOE-DYLAN), daily-scale samples  
335 of 250 mL were analyzed for dissolved and particulate  $^{232}\text{Th}$ . Sample size required combining  
336 the samples from 2-4 days for dissolved  $^{232}\text{Th}$ , contributing to some temporal smoothing.  
337 Dissolved concentrations ranged from 45-90 fmol/kg (Fig. 4C). Particulate  $^{232}\text{Th}$ , although  
338 measured at a higher, daily resolution, had a higher range of variability, from 10-290 fmol/kg. Of  
339 the total seawater  $^{232}\text{Th}$  (dissolved + particulate) during HOE-DYLAN, on average 42% was in  
340 the particulate phase (range 26-66%). This fraction particulate is higher than that for  $^{230}\text{Th}$   
341 (~15%, Roy-Barman et al., 1996) since particulate  $^{232}\text{Th}$  represents both adsorbed Th and  
342 structural Th in mineral dust.

343 The decadal time-series observations (1994-2014) of total  $^{232}\text{Th}$  (Fig. 4A) exhibit a range  
344 in concentration (~50-300 fmol/kg) that is consistent with the higher frequency observations of  
345 particulate Th in 2012-2013. Since most of the data fall within the range of 50-150 fmol/kg, we  
346 are not fully confident in the five observations of elevated concentrations (150-300 fmol/kg)  
347 observed in 1994, 1998, and 1999 samples. In particular, the 1998 and 1999 samples were  
348 collected using the moored MITESS units, as discussed in section 3.2. Mooring-collected water

349 at times had higher Th concentrations than contemporaneous ship-based sampling (Fig. 4) and  
350 thus the possibility of contamination during sampling, sample storage, or sample analysis cannot  
351 be fully discounted. In fact, the variable 1994 results from Roy-Barman et al. (1996) came from  
352 multiple samples collected on the same Niskin bottle cast. Spatial variability, related to  
353 mesoscale eddies, is another potential source of rapid changes in surface  $^{232}\text{Th}$  concentration.  
354 Conservatively excluding the elevated observations  $>150$  fmol/kg, no significant temporal term  
355 trend can be derived.

356 When all observations are placed on a monthly axis (Fig. 4B), there is little indication of  
357 elevated surface  $^{232}\text{Th}$  concentrations during the spring (Mar-Jun) season of Asian dust transport  
358 over the North Pacific. It appears that dissolved  $^{232}\text{Th}$  may be relatively constant throughout the  
359 year, consistent with the Th residence times of  $\sim 2$  yrs derived in section 4.2. Unfortunately, few  
360 observations of dissolved  $^{232}\text{Th}$  have been yet made during the spring season when dust input can  
361 increase by 2 orders of magnitude (Hyslop et al., 2013). Of course, these data are sparse, but they  
362 do provide a baseline of variability against which future trace metal observations can be  
363 measured.

#### 364 *4.4 Fe/Th ratio behavior in surface water and in colloidal content*

365 Before applying the  $^{232}\text{Th}$  flux technique, comparison of the time-series behavior of Fe  
366 (Fitzsimmons et al., in review) and  $^{232}\text{Th}$  is informative in terms of relative solubility and relative  
367 removal rates (Fig. 5). This is possible because both elements have been analyzed on the same  
368 samples from HOE-DYLAN, HOE-PhoR and many of the HOT archive samples.

369 In the context of daily, monthly and decadal variability, it appears that the ratio of total  
370 and particulate  $\text{Fe}/^{232}\text{Th}$  tends to be at or above the dust-ratio of 11,040 mol/mol, while dissolved  
371  $\text{Fe}/^{232}\text{Th}$  is at or below the dust-ratio (Fig. 5A & 5B). These observations are consistent with



372 input at the dust Fe/<sup>232</sup>Th ratio and a strong sink from biological uptake for Fe. Thus, the  
373 dissolved phase is left depleted in Fe relative to <sup>232</sup>Th, while the particulate phase becomes  
374 enriched in biogenic Fe. The total Fe/Th ratio often exceeds the dust ratio as well, possibly  
375 because biogenic particulate Fe may be efficiently recycled and thus may reside in the surface  
376 longer than particulate Th. Interestingly, the samples from moored MITESS units (open symbols  
377 in Fig. 5) had Fe/Th ratios quite close to the near-crustal ratio of Asian dust. This fact does not  
378 necessarily exclude the possibility for Th contamination in these samples but does suggest any  
379 potential metal contamination was of near-crustal composition.

380         The partitioning between dissolved and total/particulate Fe/<sup>232</sup>Th centers on the dust ratio  
381 (Fig. 5C). We interpret this to mean that the relative fractional solubility of Fe and <sup>232</sup>Th ( $S_{\text{Fe/Th}}$ )  
382 is close to 1. An alternate interpretation would be that <sup>232</sup>Th is more efficiently leached from  
383 dust, leaving the particulate phase enriched in Fe/<sup>232</sup>Th and the dissolved phase depleted in  
384 Fe/<sup>232</sup>Th. However, given the known ability for phytoplankton to efficiently utilize Fe from dust  
385 sources (e.g., (Rubin et al., 2011)), the assumption of  $S_{\text{Fe/Th}} = 1$  during dissolution followed by  
386 rapid biological uptake of Fe seems more likely. It is difficult to assign a quantitative  
387 uncertainty to the relative solubility with the existing data. The measured seawater Fe/<sup>232</sup>Th  
388 ratios ( $n = 30$ ) are on average within  $54 \pm 51\%$  (1 sigma) of the Asian dust ratio. Therefore, the  
389 relative solubility is likely close to 1 with less than 50% uncertainty, but 50% could be used as a  
390 conservative uncertainty estimate ( $S_{\text{Fe/Th}} = 1 \pm 0.5$ ). Consideration of the size-partitioning of Fe  
391 and Th within the dissolved phase provides another constraint on the pathways these elements  
392 take after being released by dust. This investigation was also used as an opportunity to  
393 determine whether <sup>232</sup>Th and <sup>230</sup>Th have coherent speciation, as assumed for the <sup>232</sup>Th flux  
394 method. Figure 6 presents these results based on measurements of ultra-filtered seawater from

395 HOE-PhoR-II in September 2013. We define colloidal Th as dissolved ( $< 0.45 \mu\text{m}$ ) minus  
396 soluble ( $< 10 \text{kDa}$ ).

397 Of the measured dissolved Th, 8-25% was found in the colloidal phase ( $0.45 \mu\text{m}$ - $10 \text{kDa}$   
398  $\approx 0.01 \mu\text{m}$ ). The total Th recovery during ultrafiltration was nearly complete (88-100%),  
399 implying that this 8-25% of dissolved Th was indeed colloidal in size, not an artifact of Th  
400 sorption/loss to the ultrafiltration system. Furthermore, at least at 15 m, 130 m (DCM), and 1000  
401 m, the colloidal percentage for  $^{232}\text{Th}$  and  $^{230}\text{Th}$  agreed within the uncertainty of the  
402 measurements. This result implies coherent speciation of these thorium isotopes despite very  
403 different sources, and it supports the use of  $^{230}\text{Th}$  as a tracer for  $^{232}\text{Th}$  removal. This coherent  
404 speciation result agrees with previous measurements of the  $^{232}\text{Th}/^{230}\text{Th}$  ratio of filtered ( $< 0.2$   
405  $\mu\text{m}$ ) and ultrafiltered ( $< 1 \text{kDa}$ ) solutions from the Mediterranean Sea (Roy-Barman et al., 2002).

406 The role of colloids in Th scavenging has much history and deserves a few words of  
407 context. Early models of scavenging inferred that Th likely goes through a colloidal intermediate  
408 before being scavenged by larger, sinking particles (Honeyman et al., 1988; Honeyman and  
409 Santschi, 1989). Subsequent attempts at measuring colloidal Th focused largely on  $^{234}\text{Th}$  (see  
410 review by (Guo and Santschi, 2007)), in part due to its use in quantifying organic matter export.  
411 A generalization might be made that outside of the coastal ocean, colloidal  $^{234}\text{Th}$  was found to be  
412 a relatively small ( $< 15\%$ ) proportion of the total dissolved (e.g., (Guo et al., 1997; Huh and  
413 Prahl, 1995; Moran and Buesseler, 1992)), which is also consistent with our  $^{230}\text{Th}$  and  $^{232}\text{Th}$   
414 results. Recent observations from the North Atlantic (Hayes et al., 2015b), however, observed  
415 scavenging characteristics consistent with a strong role for Th colloids as predicted by the  
416 “colloidal pumping hypothesis” of Honeyman and Santschi (1989), even at open-ocean particle

417 concentrations of  $< 10 \mu\text{g}/\text{kg}$  seawater. Further observations on the geographic distribution of  
418 colloidal Th are clearly warranted.

419 Our paired observations of Th and Fe size partitioning nonetheless provide additional  
420 information on their physicochemical speciation in a comparative sense. Dissolved Fe has a  
421 much higher colloidal content at ALOHA than Th (Fig. 6). Above the DCM, dissolved Fe can be  
422  $>50\%$  colloidal. In the deeper water column, to 1.5 km depth, colloidal Fe is relatively constant  
423 at 40% (with the exception of one sample  $< 10\%$  colloidal at 650 m). Since Fe and  $^{232}\text{Th}$  are  
424 apparently solubilized from dust with equal fractional solubility, this difference in size-speciation  
425 is most likely also due to the selective uptake or complexation of Fe by organic substrates.  
426 Ligands, in the form of macromolecular organic molecules or organic colloidal particles, most  
427 likely complex Fe released from dust quite rapidly in the upper water column (Bressac and  
428 Guieu, 2013; Mendez et al., 2010). We hypothesize that organic Fe-binding ligands are  
429 predominantly responsible for converting such a large percentage of dissolved Fe to colloidal  
430 size. The inorganic speciation of Th in seawater is largely hydroxo- complexes (Santschi et al.,  
431 2006). Other similarly hydrolyzable metals such as Al and Ti do not have significant colloidal  
432 components (Dammshäuser and Croot, 2012).

433 Similar to Al and Ti, the abundance of colloidal ligands ( $>10 \text{ kDa}$ ) with an affinity to  
434 complex Th must also be small compared to the source of dissolved Th from dust. This finding  
435 does not necessarily contradict previous evidence for significant organic complexation of Th in  
436 seawater (Santschi et al., 2006). It does require, however, that any significant Th complexation is  
437 done by small ( $<10 \text{ nm}$ ), low-molecular weight organic molecules, at least in the subtropical  
438 North Pacific.

439 Greater uptake of Fe into the colloidal phase is another piece of evidence that suggests  
440 that dissolved Fe is cycled more rapidly than Th in the upper water column. The innovation of  
441 the  $^{232}\text{Th}$  flux method is our ability to be quantitative about the rates of Fe removal, which are  
442 presented in the next section.

#### 443 *4.5 Iron residence times*

444 Using the 2012-2013  $^{230}\text{Th}$  profile data, we extend our calculations for Th residence time  
445 down to 1.5 km water depth in Fig. 7A. The average residence time for the depth zone between  
446 the surface and the DCM is 1-2 years. The Th residence times increase nearly linearly with  
447 integration depth to 14 years for the average residence time between the surface and 1.5 km. We  
448 do not plot integrated values shallower than the DCM (~120 m) on the assumption that steady-  
449 state Th scavenging may not apply under the conditions of stronger mixing and organic matter  
450 export within the euphotic zone. Dividing the integrated dissolved  $^{232}\text{Th}$  inventories by these  
451 residence times gives our estimate of dissolved  $^{232}\text{Th}$  flux, as a function of integration depth, in  
452 Fig. 7B.

453 In June and Sept. 2013, the dissolved  $^{232}\text{Th}$  flux increased with integration depth and  
454 began to level-off around 500 m. This pattern reflects that, at these times, the inventory of  
455 dissolved  $^{232}\text{Th}$  increased with integration depth slightly more quickly than the increase in Th  
456 residence time with depth. Interestingly, in July 2012, the dissolved  $^{232}\text{Th}$  flux decreased with  
457 integration depth, reflecting that the Th residence time increased more quickly than the dissolved  
458  $^{232}\text{Th}$  inventory, essentially because the mixed layer  $^{230}\text{Th}$  concentrations were exceptionally low  
459 at this time. Estimated  $^{232}\text{Th}$  fluxes are clearly quite sensitive to short-term variability in  
460 scavenging rates. We suggest further time-series analysis along with modelling efforts that  
461 contain circulation and realistic particle fluxes to determine more quantitatively the sensitivities

462 involved in calculating dissolved  $^{232}\text{Th}$  fluxes during moderate changes in scavenging rates and  
463 dust input.

464 The three flux profiles converge around 1000 m depth. This is encouraging that over  
465 longer integration times, 10-15 years in this case, we estimate consistent lithogenic metal fluxes  
466 at multiple time points. Using Eq. 1, the dissolved  $^{232}\text{Th}$  fluxes are simply converted to dust-  
467 dissolved Fe fluxes, using  $S_{\text{Fe/Th}} = 1$  and  $(\text{Fe/Th})_{\text{dust}} = 11,040 \text{ mol/mol}$ , shown in the second x-  
468 axis in Fig. 7B. The depth profiles of dissolved Fe concentrations from the same sampling  
469 campaigns are shown in Fig. 7C (Fitzsimmons et al., in review). Finally, using Eq. 2, by  
470 integrating Fe inventories and dividing by the dust-dissolved Fe fluxes, we estimate the residence  
471 time of dissolved Fe, as a function of integrated depth in Fig. 7D.

472 In the upper 250 m, the residence time of dissolved Fe is 6 months to 1 year, again  
473 assuming that the sole source of Fe to the surface ocean at Station ALOHA is aerosol dust  
474 deposition. This range agrees well with the 6 month residence time estimated previously at  
475 Station ALOHA (Boyle et al., 2005), and with other estimates of surface ocean dissolved Fe  
476 residence times from the Atlantic based on measured Fe concentrations and assumptions about  
477 soluble aerosol deposition (Bergquist and Boyle, 2006; Jickells, 1999; Ussher et al., 2013). With  
478 such fast turnover times, dissolved Fe concentrations in surface waters can be expected to vary  
479 on monthly to yearly timescales with changes in the seasonal input of dust from Asia. This is in  
480 fact exactly what was observed over the HOT and HOE time-series (Fitzsimmons et al., in  
481 review).

482 Available aerosol data suggest that Asian dust transport over the North Pacific had no  
483 significant long-term trend from 1981 to 2000 (Prospero et al., 2003) and perhaps a 6% decline  
484 over the past 10 years (Hyslop et al., 2013). Because of a nearly immediate impact on surface

485 water Fe concentrations and the associated ecological consequences, it is important to monitor  
486 future changes in Fe sources. Sources such as Asian desert dust in our changing climate may  
487 vary independently of other Fe sources such as combustion aerosols.

488         As one integrates further from 250 m to 1500 m, while the dissolved Fe fluxes change  
489 only moderately, the dissolved Fe residence times increase quickly to about 10 years at 1500 m  
490 depth. This is due to the large increase in Fe concentrations at these depths due to  
491 remineralization of Fe from sinking organic material and some portion of Fe accumulated and  
492 transported to ALOHA laterally via deep ocean circulation. There is potentially additional input  
493 of Fe at ~1 km depth due to Loihi hydrothermal activity. Additional lateral sources would cause  
494 our dust-based dissolved Fe residence time to be an overestimate, implying even faster  
495 timescales of Fe removal. On the other hand, as discussed in the next section, the 10 year Fe  
496 residence time at 1500 m could as well be an underestimate, if the geochemical cycles of Th and  
497 Fe become decoupled at greater depths where dust dissolution is no longer the most significant  
498 source of dissolved Fe.

#### 499         *4.6 Fe and Th decoupling in the deep ocean*

500         Our focus on the upper water column stems from our motivation to understand trace  
501 metal cycling due to aerosol deposition and export production. We can extend our analysis of Fe  
502 and Th into the deep ocean (4.5 km water depth at Station ALOHA) to learn about the  
503 geochemistry of these elements over decadal-to-centennial timescales. In Figure 8, we compiled  
504 available deep profiles from Station ALOHA for dissolved Fe (Boyle et al., 2005; Fitzsimmons  
505 et al., in review; Morton, 2010) and dissolved  $^{232}\text{Th}$  and  $^{230}\text{Th}$  (this study; Roy-Barman et al.  
506 (1996)).

507 Variability in dissolved Fe at 1-1.5 km is clearly apparent, likely due to hydrothermal  
508 inputs. Below 1.5 km depth, Fe,  $^{232}\text{Th}$ , and  $^{230}\text{Th}$  display relatively constant profile shapes, at  
509 least during the sparse sampling dates. From 2 km depth to the bottom, dissolved Fe is nearly  
510 constant or slightly decreases with depth to about 0.4 nmol/kg, while dissolved  $^{232}\text{Th}$  actually  
511 increases with depth from 50 to 180 fmol/kg below 3000 m. This divergence in profile shape  
512 already suggests a decoupling of the behavior of these elements in the deep ocean.

513 The deep ocean appears to contain an additional source for  $^{232}\text{Th}$ . This source is  
514 potentially related to resuspension of diagenetically-altered sediments at the seafloor (Hayes et  
515 al., 2013a; Okubo et al., 2012). The bottom-increase in  $^{232}\text{Th}$  begins nearly 2 km above the  
516 seafloor, much higher than typical benthic vertical mixed layers (50-100 m) (Richards, 1990).  
517 This phenomenon, as observed with km-scale nepheloid layers (McCave, 1986), suggests that  
518 the  $^{232}\text{Th}$  at abyssal depths of Station ALOHA is being mixed in laterally from locations where  
519 isopycnals impinge on surrounding bathymetry.

520 Also related to bottom sediment resuspension, the July 2012 profile of  $^{230}\text{Th}$  displays a  
521 negative concentration anomaly, or deficit of  $^{230}\text{Th}$ , with respect to the linear profile near the  
522 seafloor (Fig. 8C). This bottom  $^{230}\text{Th}$  deficit is indicative of enhanced bottom scavenging as  
523 observed in many parts of the deep North Pacific (Hayes et al., 2013b; Okubo et al., 2012). It is  
524 non-intuitive that a bottom layer where the scavenging removal of Th is enhanced compared to  
525 the overlaying water column would also be a strong source of  $^{232}\text{Th}$ . The resuspension of bottom  
526 sediments may produce such a strong release of  $^{232}\text{Th}$  that this source more than compensates for  
527 enhanced scavenging. Another contributing factor may be that the resuspended thorium could  
528 have a much higher  $^{232}\text{Th}/^{230}\text{Th}$  ratio than the water column due to age-decay of  $^{230}\text{Th}$  in the  
529 sediments.

530           Dissolved Fe, on the other hand, appears unaffected by bottom processes, displaying only  
531 a slight decrease in concentration with depth (Fig. 8A). The slight decrease with depth may be  
532 related to scavenging of Fe as deep water masses age (Bruland et al., 1994). If we extend our  
533 integrated residence time approach to the deep Fe profile at Station ALOHA (Fig. 9), we derive a  
534 whole ocean residence for dissolved Fe of only 30 years. This is significantly shorter than the  
535 100-300 year estimates of the ocean residence time for dissolved Fe based on deepwater  
536 scavenging (Bergquist and Boyle, 2006; Bruland et al., 1994). This discrepancy must arise  
537 because the deep ocean source of  $^{232}\text{Th}$  does not add dissolved Fe to the water column at a  
538 crustal ratio, unlike what occurs during near-surface dust dissolution. Thus, the  $^{232}\text{Th}$  flux  
539 method for Fe residence times probably should not be extended to the deep ocean.

540           The question remains: how is an element like Th, a trace component of continental  
541 material, added to the deep ocean without a simultaneous release of a major crustal element like  
542 Fe? The answer is likely related to solubility.

543           Dissolved Fe in the deep central North Pacific at  $\sim 0.5$  nmol/kg has been found to be at  
544 near solubility equilibrium with Fe(III) hydroxide (Kitayama et al., 2009; Kuma et al., 2003).  
545 These studies determine Fe(III) solubility by adding gamma-emitter  $^{59}\text{Fe(III)}$  to filtered seawater,  
546 allowing the solutions to come to solubility equilibrium with Fe(III) hydroxide over several  
547 weeks, subsequently filtering the seawater and then counting the  $^{59}\text{Fe}$  gamma-activity on the  
548 final filtrate. The observed  $\sim 0.5$  nmol/kg solubility is elevated over Fe solubility in inorganic  
549 seawater because of the presence of organic ligands (Liu and Millero, 2002). Thus, since the  
550 deep Pacific is in a near saturation state, dissolved Fe can no longer be expected to increase, even  
551 in the presence of increasing Th concentrations.



552 A problem with this argument is that electrochemically-determined Fe ligand  
553 concentrations at Station ALOHA are up to 2 nmol/kg, well in excess of dissolved Fe  
554 concentrations (Rue and Bruland, 1995), as found in most of the world ocean (Gledhill and  
555 Buck, 2012). However, it may not be kinetically appropriate to compare Fe ligand concentrations  
556 directly with seawater solubility. In either estimation, deepwater dissolved Fe is at least close to  
557 (within the same order of magnitude) our best estimates of Fe solubility.

558 While much less is known about Th solubility in seawater, our large underestimate of Fe  
559 residence time in the deep ocean implies that the deep North Pacific, with Th at ~180 fmol/kg, is  
560 below Th solubility equilibrium. Near seawater pH and ionic strength, the solubility of Th(IV)  
561 hydroxide may be as high as 0.5-1 nmol/kg, compared to 1 fmol/kg for crystalline ThO<sub>2</sub>, due to  
562 the amorphous nature of Th(OH)<sub>4</sub> solids (Neck et al., 2003). Also, electrochemical methods  
563 suggest organic Th ligands exist at nanomolar concentrations (Hirose, 2004). Despite our finding  
564 of low colloidal Th content, organically-bound Th could of course be present at Station ALOHA  
565 if the complexes are smaller than ~10 nm. We advocate direct measurements of Th solubility in  
566 seawater, perhaps using radio-tracer additions with similar protocols as developed for Fe (Kuma  
567 et al., 1996; Schlosser and Croot, 2008), to confirm that Th exists in the deep ocean at much less  
568 than its equilibrium solubility. This would explain the fact that dissolved Th concentrations  
569 continue to grow from lithogenic sources in the deep North Pacific, where Fe concentrations  
570 become fixed by a solubility limit.

## 571 **5. Conclusions**

572 Using time-series data from the North Pacific, this study finds variability in surface Fe  
573 and <sup>232</sup>Th concentrations consistent with a source from Asian dust. The dust source likely has a  
574 relative Fe/Th fractional solubility close to 1. The application of <sup>230</sup>Th scavenging rates to <sup>232</sup>Th

575 inventories allows the accurate evaluation of the flux of dissolved metals from dust in the remote  
576 surface ocean. The source flux of dissolved Fe, derived from  $^{230}\text{Th}$ -based timescales, suggests  
577 that dissolved Fe in the upper 250 m is turning over in 1 year or less. A compelling implication  
578 of this result is that Fe delivery to phytoplankton can be expected to vary with seasonal-to-  
579 interannual changes in dust delivery from Asia. Continued monitoring of Fe-dependent  
580 biological processes, such as nitrogen fixation, are crucial to anticipate the consequences of  
581 changing land-use and/or industrial processes that may significantly affect eolian sources of Fe  
582 to the North Pacific.

583         In addition, by comparing Fe and Th size-partitioning, we find evidence that colloidal Fe  
584 may be of predominantly organic composition in the subtropical North Pacific. We also  
585 hypothesize that iron reaches a solubility limit in the deep sea (>2 km) while Th does not. While  
586 less controversial for Th, this result questions the relevance of “excess” Fe ligands in the deep  
587 sea. Overall, however, the kinetic box model approach to tracing dust-derived elements (Fig. 1)  
588 appears well-suited in the upper water column (~250 m).

### 589 **Acknowledgements**

590 We acknowledge funding from the W.O. Crosby Postdoctoral Fellowship to CTH and the  
591 National Science Foundation through C-MORE, NSF-OIA EF-0424599 to EAB, and NSF-DMR  
592 1157490 supported RW and PLM. Soumen Mallick and Alberto Saal are thanked for facilitating  
593 mass spectrometry performed at Brown University. Major thanks go to Tara Clemente and Sam  
594 Wilson for their leadership roles on C-MORE cruises, and to Rick Kayser, Gonzalo Carrasco,  
595 Abigail Noble, Simone Moos, Mengli Chen, and Rene Boiteau for their help in collecting  
596 samples returned to MIT. The associate editor, Timothy Shaw, an anonymous reviewer, and  
597 Michiel Rutgers van der Loeff are thanked for their constructive evaluations of the manuscript.

598

### 599 **Figure Captions**

600 **Figure 1.** Tracing the Fe cycle with the behavior of the long-lived thorium isotopes. Thorium-  
 601 <sup>230</sup>Th has a well-known source from the radioactive decay of its parent <sup>234</sup>U. This allows a  
 602 quantitative estimate of Th removal due to scavenging on to particles. This removal rate can be  
 603 used to estimate the steady-state source of <sup>232</sup>Th from the partial dissolution of aerosol dust,  
 604 assuming dust dissolution and scavenging dominate the Th cycle which may be most relevant in  
 605 the remote surface ocean. While Fe has many more terms in its biogeochemical cycling, its  
 606 ultimate source from dust dissolution can be predicted using known <sup>232</sup>Th fluxes and the relative  
 607 solubility of Fe and Th. Assuming Fe is derived only from dust, one can then estimate a  
 608 maximum Fe residence time or minimum turnover rate.

609  
 610 **Figure 2.** Depth profiles from the Hawaii Ocean Time-series Station ALOHA from sampling  
 611 campaigns in 2012-2013. In July 2012 and June 2013, profiles for dissolved <sup>232</sup>Th (A) and <sup>230</sup>Th  
 612 (B) were collected in two casts (shallow to 250 m and deep to 1500 m) on different days.  
 613 Relative uncertainty in isotope concentrations was 1-5% and thus errors bars would be close to  
 614 the symbol size. The hydrographic profiles (C-F) are shown from the shallow cast only.

615  
 616 **Figure 3.** Thorium residence times, or turnover rates, calculated for the upper 150 m at Station  
 617 ALOHA on a monthly axis combining data from 1999 to 2014. These times are calculated by  
 618 comparing integrated Th inventories to integrated production by uranium decay. The <sup>234</sup>Th-based  
 619 results are reported by Buesseler et al. (2009) and Benitez-Nelson et al. (2001). Note the <sup>230</sup>Th-  
 620 based results from March 2014 are not based on profiles but on single samples from 25 m,  
 621 assuming uniform concentrations in the upper 150 as seen in the 2012-2013 profiles (Fig. 2).

622  
 623 **Figure 4.** Station ALOHA time-series data from the surface ocean (0-10 meters depth) on  
 624 dissolved (filtered at 0.45 or 0.4  $\mu$ m), total (unfiltered) and particulate (digested 0.4  $\mu$ m filter)  
 625 <sup>232</sup>Th in full time-series (1994-2014) (A), monthly climatology (1991-2014) (B) and during a  
 626 daily resolution period in July-Sept. 2012 (C). Note change in scale of y-axes at 160 fmol/kg.  
 627 Results from 1994 were reported by Roy-Barman et al. (1996). Open circles represent samples  
 628 collected using a mooring rather than ship-based sampling (Sec. 4.1). Relative uncertainty in  
 629 dissolved, total and particulate <sup>232</sup>Th concentrations was 1-10%.

630  
 631 **Figure 5.** Station ALOHA time-series data from the surface ocean (0-10 meters depth) (A),  
 632 monthly climatology (B) and a daily resolution period in July-Sept. 2012 (C) of the dissolved  
 633 (filtered at 0.45 or 0.4  $\mu$ m), total (unfiltered) and particulate (digested 0.4  $\mu$ m filter) Fe/<sup>232</sup>Th  
 634 ratio. Note change in scale of y-axes at 25,000 mol/mol. The dotted lines represent the Fe/<sup>232</sup>Th  
 635 ratio of Asian dust of  $10,800 \pm 1,200$  mol/mol ( $1\sigma$ ). Note in (C), four samples with particulate  
 636 Fe/<sup>232</sup>Th ratios greater than 40,000 are not shown. Open circles represent samples collected using  
 637 a mooring rather than ship-based sampling (Sec. 4.1).

638  
 639 **Figure 6.** Depth profiles of the percentage of dissolved metals (<0.45  $\mu$ m for Th or <0.4  $\mu$ m for  
 640 Fe) that are in the colloidal size fraction (roughly 10-400 nm) from Station ALOHA in late  
 641 September 2013. Colloidal content is estimated by subtracting the metal concentration in 0.4  $\mu$ m  
 642 filtered seawater (dissolved) from that passing through a 10 kDa membrane filter by cross-flow  
 643 filtration (soluble). Colloidal fractions of <sup>232</sup>Th and <sup>230</sup>Th agree within uncertainties, while Fe  
 644 colloidal content is 2-3 times larger.

645  
 646 **Figure 7.** Application of dissolved  $^{232}\text{Th}$  fluxes to predict the residence time of dissolved Fe in  
 647 seawater at Station ALOHA during 2012-2013. Dissolved Th residence times (A) are calculated  
 648 as a function of integration depth using radioactive disequilibrium between  $^{234}\text{U}$  and  $^{230}\text{Th}$ .  
 649 Integrated values shallower than the deep chlorophyll maximum (~120 m) are not included on  
 650 the assumption that steady-state Th scavenging may not apply within the euphotic zone. The  
 651 integrated  $^{232}\text{Th}$  inventories divided by these residence times produces an estimate of the  
 652 dissolved  $^{232}\text{Th}$  flux (B) due to dust dissolution. Assuming equal fractional solubilities  
 653 dissolution and a near crustal composition for Asian dust, the flux of dissolved Fe from dust can  
 654 be predicted using the second x-axis in (B). The integration of dissolved Fe inventories based on  
 655 concentration profiles shown in (C) (Fitzsimmons et al., in review), produces our estimate of  
 656 dissolved Fe residence time in (D, note change in scale of x-axis at 1.2 yrs).

657  
 658 **Figure 8.** Full ocean depth profiles from Station ALOHA for dissolved Fe (A),  $^{232}\text{Th}$  (B) and  
 659  $^{230}\text{Th}$  (C) using data from this study (July 2012) and compiled from the literature. Iron data from  
 660 April 2001 and July 2002 were reported by Boyle et al. (2005) and from June 2002 by Morton  
 661 (2010). Dissolved Th data from 1994 were reported by Roy-Barman et al. (1996). Note in (C) the  
 662 dotted grey line is the linear regression of  $^{230}\text{Th}$  data between 1 and 3.5 km, which when  
 663 extended to the seafloor demonstrates that the bottom two samples are less than expected from  
 664 reversible scavenging and imply enhanced scavenging (assuming no other processes affect  
 665 supply and removal of  $^{230}\text{Th}$  here).

666  
 667 **Figure 9.** Application of dissolved  $^{232}\text{Th}$  fluxes to predict Fe residence times for the full depth  
 668 ocean at Station ALOHA. Here data from July 2012 are used to calculate  $^{232}\text{Th}$  fluxes (A). The  
 669 depth profiles of Fe concentrations presented in Fig. 8 were averaged to calculate the dissolved  
 670 Fe residence times as a function of integration depth (B). The 30 year ocean residence for  
 671 dissolved Fe is significantly lower than the century-scale residence times derived by other  
 672 approaches, suggesting that  $^{232}\text{Th}$  flux may not be an accurate proxy for Fe sources in the deep  
 673 ocean.

#### 674 References

- 675  
 676  
 677 Andersen, M.B., Stirling, C.H., Zimmermann, B. and Halliday, A.N. (2010) Precise determination of the  
 678 open ocean  $^{234}\text{U}/^{238}\text{U}$  composition. *Geochem. Geophys. Geosyst.* 11, Q12003.
- 679 Anderson, R.F., Fleisher, M.Q., Robinson, L.F., Edwards, R.L., Hoff, J., Moran, S.B., Rutgers van der  
 680 Loeff, M.M., Thomas, A.L., Roy-Barman, M. and François, R. (2012) GEOTRACES intercalibration of  
 681  $^{230}\text{Th}$ ,  $^{232}\text{Th}$ ,  $^{231}\text{Pa}$ , and prospects for  $^{10}\text{Be}$ . *Limnol. Oceanogr. Methods* 10, 179-213.
- 682 Andersson, P.S., Wasserburg, G.J., Chen, J.H., Papanastassiou, D.A. and Ingri, J. (1995)  $^{238}\text{U}$ - $^{234}\text{U}$  and  
 683  $^{232}\text{Th}$ - $^{230}\text{Th}$  in the Baltic Sea and in river water. *Earth Planet. Sci. Lett.* 130, 217-234.
- 684 Auro, M.E., Robinson, L.F., Burke, A., Bradtmiller, L.I., Fleisher, M.Q. and Anderson, R.F. (2012)  
 685 Improvements to  $^{232}\text{Th}$ ,  $^{230}\text{Th}$ , and  $^{231}\text{Pa}$  analysis in seawater arising from  
 686 GEOTRACES intercalibration. *Limnol. Oceanogr. Methods* 10, 464-474.

- 687 Bacon, M.P. and Anderson, R.F. (1982) Distribution of thorium isotopes between dissolved and  
688 particulate forms in the deep sea. *J. Geophys. Res.* 87, 2045-2056.
- 689 Barbeau, K., Kujawinski, E.B. and Moffett, J.W. (2001) Remineralization and recycling of iron, thorium  
690 and organic carbon by heterotrophic marine protists in culture. *Aquat. Microb. Ecol.* 24, 69-81.
- 691 Barone, B., Bidigare, R.R., Church, M.J., Karl, D.M., Letelier, R.M. and White, A.E. (2015) Particle  
692 distributions and dynamics in the euphotic zone of the North Pacific Subtropical Gyre. *Journal of*  
693 *Geophysical Research: Oceans*, Available online <http://dx.doi.org/10.1002/2015JC010774>.
- 694 Bell, J., Betts, J. and Boyle, E. (2002) MITESS: a moored in situ trace element serial sampler for deep-sea  
695 moorings. *Deep-Sea Res. I* 49, 2103-2118.
- 696 Benitez-Nelson, C., Buesseler, K.O., Karl, D.M. and Andrews, J. (2001) A time-series study of  
697 particulate matter export in the North Pacific Subtropical Gyre based on  $^{234}\text{Th}$ : $^{238}\text{U}$  disequilibrium. *Deep-*  
698 *Sea Res. I* 48, 2595-2611.
- 699 Bergquist, B.A. and Boyle, E.A. (2006) Dissolved iron in the tropical and subtropical Atlantic Ocean.  
700 *Global Biogeochem. Cycles* 20, GB1015.
- 701 Bishop, J.K.B. and Wood, T.J. (2008) Particulate matter chemistry and dynamics in the twilight zone at  
702 VERTIGO, ALOHA and K2 sites. *Deep-Sea Res. I* 55, 1684-1706.
- 703 Boyd, P.W., Mackie, D.S. and Hunter, K.A. (2010) Aerosol iron deposition to the surface ocean —  
704 Modes of iron supply and biological responses. *Mar. Chem.* 120, 128-143.
- 705 Boyle, E.A., Bergquist, B.A., Kayser, R.A. and Mahowald, N. (2005) Iron, manganese, and lead at  
706 Hawaii Ocean Time-series station ALOHA: Temporal variability and an intermediate water hydrothermal  
707 plume. *Geochim. Cosmochim. Acta* 69, 933-952.
- 708 Bressac, M. and Guieu, C. (2013) Post-depositional processes: What really happens to new atmospheric  
709 iron in the ocean's surface? *Global Biogeochem. Cycles* 27, 859-870.
- 710 Bruland, K.W., Orians, K.J. and Cowen, J.P. (1994) Reactive trace metals in the stratified central North  
711 Pacific. *Geochim. Cosmochim. Acta* 58, 3171-3182.
- 712 Buesseler, K.O., Bacon, M.P., Kirk Cochran, J. and Livingston, H.D. (1992) Carbon and nitrogen export  
713 during the JGOFS North Atlantic Bloom experiment estimated from  $^{234}\text{Th}$ : $^{238}\text{U}$  disequilibria. *Deep-Sea*  
714 *Res. A* 39, 1115-1137.
- 715 Buesseler, K.O., Pike, S., Maiti, K., Lamborg, C.H., Siegel, D.A. and Trull, T.W. (2009) Thorium-234 as  
716 a tracer of spatial, temporal and vertical variability in particle flux in the North Pacific. *Deep-Sea Res. I*  
717 56, 1143-1167.
- 718 Charette, M.A., Breier, C.F., Henderson, P.B., Pike, S.M., Rypina, I.I., Jayne, S.R. and Buesseler, K.O.  
719 (2013) Radium-based estimates of cesium isotope transport and total direct ocean discharges from the  
720 Fukushima Nuclear Power Plant accident. *Biogeosciences* 10, 2159-2167.
- 721 Cheng, H., Edwards, R.L., Shen, C.-C., Polyak, V.J., Asmerom, Y., Woodhead, J., Hellstrom, J., Wang,  
722 Y., Kong, X., Spötl, C., Wang, X. and Calvin Alexander Jr, E. (2013) Improvements in  $^{230}\text{Th}$  dating,  $^{230}\text{Th}$

- 723 and  $^{234}\text{U}$  half-life values, and U–Th isotopic measurements by multi-collector inductively coupled plasma  
724 mass spectrometry. *Earth Planet. Sci. Lett.* 371–372, 82-91.
- 725 Church, M.J., Lomas, M.W. and Muller-Karger, F. (2013) Sea change: Charting the course for  
726 biogeochemical ocean time-series research in a new millennium. *Deep-Sea Res. II* 93, 2-15.
- 727 Coale, K.H. and Bruland, K.W. (1985)  $^{234}\text{Th}$ : $^{238}\text{U}$  disequilibria within the California Current. *Limnol.*  
728 *Oceanogr.* 30, 22-33.
- 729 Conway, T.M. and John, S.G. (2014) Quantification of dissolved iron sources to the North Atlantic  
730 Ocean. *Nature* 511, 212-215.
- 731 Dammshäuser, A. and Croot, P.L. (2012) Low colloidal associations of aluminium and titanium in surface  
732 waters of the tropical Atlantic. *Geochim. Cosmochim. Acta* 96, 304-318.
- 733 Dammshäuser, A., Wagener, T., Garbe-Schönberg, D. and Croot, P. (2013) Particulate and dissolved  
734 aluminum and titanium in the upper water column of the Atlantic Ocean. *Deep-Sea Res. I* 73, 127-139.
- 735 Deng, F., Thomas, A.L., Rijkenberg, M.J.A. and Henderson, G.M. (2014) Controls on seawater  $^{231}\text{Pa}$ ,  
736  $^{230}\text{Th}$  and  $^{232}\text{Th}$  concentrations along the flow paths of deep waters in the Southwest Atlantic. *Earth*  
737 *Planet. Sci. Lett.* 390, 93-102.
- 738 Edwards, R.L., Chen, J.H. and Wasserburg, G.J. (1987)  $^{238}\text{U}$ - $^{234}\text{U}$ - $^{230}\text{Th}$ - $^{232}\text{Th}$  systematics and the precise  
739 measurement of time over the past 500,000 years. *Earth Planet. Sci. Lett.* 81, 175-192.
- 740 Fitzsimmons, J.N. and Boyle, E.A. (2014a) Assessment and comparison of Anopore and cross flow  
741 filtration methods for the determination of dissolved iron size fractionation into soluble and colloidal  
742 phases in seawater. *Limnol. Oceanogr. Methods* 12, 246-263.
- 743 Fitzsimmons, J.N. and Boyle, E.A. (2014b) Both soluble and colloidal iron phases control dissolved iron  
744 variability in the tropical North Atlantic Ocean. *Geochim. Cosmochim. Acta* 125, 539-550.
- 745 Fitzsimmons, J.N., Hayes, C.T., al-Subiai, S., Morton, P.L., Weisend, R., Ascani, F. and Boyle, E.A. (in  
746 review) Daily to decadal variability of size-fractionated iron and iron-binding ligands at the Hawaii Ocean  
747 Time-series Station ALOHA. *Geochim. Cosmochim. Acta*.
- 748 Gledhill, M. and Buck, K.N. (2012) The organic complexation of iron in the marine environment: A  
749 review. *Front. Microbiol.* 3.
- 750 Guo, L. and Santschi, P.H. (2007) Ultrafiltration and its applications to sampling and characterisation of  
751 aquatic colloids. *IUPAC Series on Analytical and Physical Chemistry of Environmental Systems* 10, 159.
- 752 Guo, L., Santschi, P.H. and Baskaran, M. (1997) Interactions of thorium isotopes with colloidal organic  
753 matter in oceanic environments. *Colloids Surf. A* 120, 255-271.
- 754 Hayes, C.T., Anderson, R.F., Fleisher, M.Q., Huang, K.-F., Robinson, L.F., Lu, Y., Cheng, H., Edwards,  
755 R.L. and Moran, S.B. (2015a)  $^{230}\text{Th}$  and  $^{231}\text{Pa}$  on GEOTRACES GA03, the U.S. GEOTRACES North  
756 Atlantic transect, and implications for modern and paleoceanographic chemical fluxes. *Deep-Sea Res. II*  
757 116, 29-41.

- 758 Hayes, C.T., Anderson, R.F., Fleisher, M.Q., Serno, S., Winckler, G. and Gersonde, R. (2013a)  
759 Quantifying lithogenic inputs to the North Pacific Ocean using the long-lived thorium isotopes. *Earth*  
760 *Planet. Sci. Lett.* 383, 16-25.
- 761 Hayes, C.T., Anderson, R.F., Fleisher, M.Q., Vivancos, S.M., Lam, P.J., Ohnemus, D.C., Huang, K.-F.,  
762 Robinson, L.F., Lu, Y., Cheng, H., Edwards, R.L. and Moran, S.B. (2015b) Intensity of Th and Pa  
763 scavenging partitioned by particle chemistry in the North Atlantic Ocean. *Marine Chemistry* 170, 49-60.
- 764 Hayes, C.T., Anderson, R.F., Jaccard, S.L., François, R., Fleisher, M.Q., Soon, M. and Gersonde, R.  
765 (2013b) A new perspective on boundary scavenging in the North Pacific Ocean. *Earth Planet. Sci. Lett.*  
766 369-370, 86-97.
- 767 Hirose, K. (2004) Chemical Speciation of Thorium in Marine Biogenic Particulate Matter.  
768 *TheScientificWorldJOURNAL* 4, 67-76.
- 769 Hirose, K. and Tanoue, E. (1994) Thorium-particulate matter interaction. Thorium complexing capacity  
770 of oceanic particulate matter: Theory. *Geochim. Cosmochim. Acta* 58, 1-7.
- 771 Ho, T.-Y., Chou, W.-C., Lin, H.-L. and Sheu, D.D. (2011) Trace metal cycling in the deep water of the  
772 South China Sea: The composition, sources, and fluxes of sinking particles. *Limnol. Oceanogr.* 56, 1225-  
773 1243.
- 774 Honeyman, B.D., Balistrieri, L.S. and Murray, J.W. (1988) Oceanic trace metal scavenging: the  
775 importance of particle concentration. *Deep-Sea Res. A* 35, 227-246.
- 776 Honeyman, B.D. and Santschi, P.H. (1989) A Brownian-pumping model for oceanic trace metal  
777 scavenging: Evidence from Th isotopes. *J. Mar. Res.* 47, 951-992.
- 778 Hsieh, Y.-T., Henderson, G.M. and Thomas, A.L. (2011) Combining seawater  $^{232}\text{Th}$  and  $^{230}\text{Th}$   
779 concentrations to determine dust fluxes to the surface ocean. *Earth Planet. Sci. Lett.* 312, 280-290.
- 780 Huh, C.-A. and Prahl, F.G. (1995) Role of colloids in upper ocean biogeochemistry in the northeast  
781 Pacific Ocean elucidated from  $^{238}\text{U}$ - $^{234}\text{Th}$  disequilibria. *Limnol. Oceanogr.* 40, 528-528.
- 782 Hyslop, N.P., Trzepla, K., Wallis, C.D., Matzoll, A.K. and White, W.H. (2013) Technical note: A 23-year  
783 record of twice-weekly aerosol composition measurements at Mauna Loa Observatory. *Atmos. Environ.*  
784 80, 259-263.
- 785 Jickells, T.D. (1999) The inputs of dust derived elements to the Sargasso Sea; a synthesis. *Mar. Chem.* 68,  
786 5-14.
- 787 Jickells, T.D., An, Z.S., Andersen, K.K., Baker, A.R., Bergametti, G., Brooks, N., Cao, J.J., Boyd, P.W.,  
788 Duce, R.A., Hunter, K.A., Kawahata, H., Kubilay, N., laRoche, J., Liss, P.S., Mahowald, N., Prospero,  
789 J.M., Ridgwell, A.J., Tegen, I. and Torres, R. (2005) Global iron connections between desert dust, ocean  
790 biogeochemistry, and climate. *Science* 308, 67-71.
- 791 Karl, D.M., Church, M.J., Dore, J.E., Letelier, R.M. and Mahaffey, C. (2012) Predictable and efficient  
792 carbon sequestration in the North Pacific Ocean supported by symbiotic nitrogen fixation. *Proc. Natl.*  
793 *Acad. Sci. U. S. A.*

- 794 Karl, D.M. and Lukas, R. (1996) The Hawaii Ocean Time-series (HOT) program: Background, rationale  
795 and field implementation. *Deep-Sea Res. II* 43, 129-156.
- 796 Kitayama, S., Kuma, K., Manabe, E., Sugie, K., Takata, H., Isoda, Y., Toya, K., Saitoh, S.-i., Takagi, S.,  
797 Kamei, Y. and Sakaoka, K. (2009) Controls on iron distributions in the deep water column of the North  
798 Pacific Ocean: Iron(III) hydroxide solubility and marine humic-type dissolved organic matter. *J.*  
799 *Geophys. Res.* 114, C08019.
- 800 Kuma, K., Isoda, Y. and Nakabayashi, S. (2003) Control on dissolved iron concentrations in deep waters  
801 in the western North Pacific: Iron(III) hydroxide solubility. *J. Geophys. Res.* 108, 3289.
- 802 Kuma, K., Nishioka, J. and Matsunaga, K. (1996) Controls on iron(III) hydroxide solubility in seawater:  
803 the influence of pH and natural organic chelators. *Limnol. Oceanogr.* 41, 396-407.
- 804 Lee, J.-M., Boyle, E.A., Echegoyen-Sanz, Y., Fitzsimmons, J.N., Zhang, R. and Kayser, R.A. (2011)  
805 Analysis of trace metals (Cu, Cd, Pb, and Fe) in seawater using single batch nitrilotriacetate resin  
806 extraction and isotope dilution inductively coupled plasma mass spectrometry. *Anal. Chim. Acta* 686, 93-  
807 101.
- 808 Lehnert, K., Su, Y., Langmuir, C.H., Sarbas, B. and Nohl, U. (2000) A global geochemical database  
809 structure for rocks. *Geochemistry, Geophysics, Geosystems* 1, 1012.
- 810 Liu, X. and Millero, F.J. (2002) The solubility of iron in seawater. *Mar. Chem.* 77, 43-54.
- 811 Luo, S., Ku, T.-L., Kusakabe, M., Bishop, J.K.B. and Yang, Y.-L. (1995) Tracing particle cycling in the  
812 upper ocean with  $^{230}\text{Th}$  and  $^{228}\text{Th}$ : An investigation in the equatorial Pacific along 140°W. *Deep-Sea Res.*  
813 *II* 42, 805-829.
- 814 Mahowald, N.M., Baker, A.R., Bergametti, G., Brooks, N., Duce, R.A., Jickells, T.D., Kubilay, N.,  
815 Prospero, J.M. and Tegen, I. (2005) Atmospheric global dust cycle and iron inputs to the ocean. *Global*  
816 *Biogeochem. Cycles* 19, GB4025.
- 817 Martínez-García, A., Sigman, D.M., Ren, H., Anderson, R.F., Straub, M., Hodell, D.A., Jaccard, S.L.,  
818 Eglinton, T.I. and Haug, G.H. (2014) Iron Fertilization of the Subantarctic Ocean During the Last Ice  
819 Age. *Science* 343, 1347-1350.
- 820 McCave, I.N. (1986) Local and global aspects of the bottom nepheloid layers in the world ocean. *Neth. J.*  
821 *Sea Res.* 20, 167-181.
- 822 McGee, D. (2009) Reconstructing and interpreting the dust record and probing the plumbing of Mono  
823 Lake. PhD dissert. Columbia University, New York, NY.
- 824 Mendez, J., Guieu, C. and Adkins, J. (2010) Atmospheric input of manganese and iron to the ocean:  
825 Seawater dissolution experiments with Saharan and North American dusts. *Mar. Chem.* 120, 34-43.
- 826 Moore, C.M., Mills, M.M., Arrigo, K.R., Berman-Frank, I., Bopp, L., Boyd, P.W., Galbraith, E.D.,  
827 Geider, R.J., Guieu, C., Jaccard, S.L., Jickells, T.D., La Roche, J., Lenton, T.M., Mahowald, N.M.,  
828 Maranon, E., Marinov, I., Moore, J.K., Nakatsuka, T., Oschlies, A., Saito, M.A., Thingstad, T.F., Tsuda,  
829 A. and Ulloa, O. (2013) Processes and patterns of oceanic nutrient limitation. *Nature Geosci.* 6, 701-710.



- 830 Moran, S.B. and Buesseler, K.O. (1992) Short residence time of colloids in the upper ocean estimated  
831 from  $^{238}\text{U}$ - $^{234}\text{Th}$  disequilibria. *Nature* 359, 221-223.
- 832 Morton, P.L. (2010) Trace metal biogeochemistry in the western North Pacific, PhD Dissert. Old  
833 Dominion University, Norfolk, VA.
- 834 Morton, P.L., Landing, W.M., Hsu, S.-C., Milne, A., Aguilar-Islas, A.M., Baker, A.R., Bowie, A.R.,  
835 Buck, C.S., Gao, Y., Gichuki, S., Hastings, M.G., Hatta, M., Johansen, A.M., Losno, R., Mead, C., Patay,  
836 M.D., Swarr, G., Vendermark, A. and Zamora, L.M. (2013) Methods for sampling and analysis of marine  
837 aerosols: results from the 2008 GEOTRACES aerosol intercalibration experiment. *Limnol. Oceanogr.*  
838 *Methods* 11, 62-78.
- 839 Neck, V., Altmaier, M., Müller, R., Bauer, A., Fanghänel, T. and Kim, J.-I. (2003) Solubility of  
840 crystalline thorium dioxide. *Radiochim. Acta* 91.
- 841 Ohnemus, D.C. and Lam, P.J. (2015) Cycling of lithogenic marine particles in the US GEOTRACES  
842 North Atlantic transect. *Deep-Sea Res. II* 116, 283-302.
- 843 Okubo, A., Obata, H., Gamo, T. and Yamada, M. (2012)  $^{230}\text{Th}$  and  $^{232}\text{Th}$  distributions in mid-latitudes of  
844 the North Pacific Ocean: Effect of bottom scavenging. *Earth Planet. Sci. Lett.* 339–340, 139-150.
- 845 Owens, S.A., Buesseler, K.O. and Sims, K.W.W. (2011) Re-evaluating the  $^{238}\text{U}$ -salinity relationship in  
846 seawater: Implications for the  $^{238}\text{U}$ - $^{234}\text{Th}$  disequilibrium method. *Mar. Chem.* 127, 31-39.
- 847 Prospero, J.M., Savoie, D.L. and Arimoto, R. (2003) Long-term record of nss-sulfate and nitrate in  
848 aerosols on Midway Island, 1981–2000: Evidence of increased (now decreasing?) anthropogenic  
849 emissions from Asia. *J. Geophys. Res.* 108, 4019.
- 850 Reuer, M.K., Boyle, E.A. and Grant, B.C. (2003) Lead isotope analysis of marine carbonates and  
851 seawater by multiple collector ICP-MS. *Chem. Geol.* 200, 137-153.
- 852 Richards, K.J. (1990) Physical processes in the benthic boundary layer. *Philos. Trans. R. Soc. London,*  
853 *Ser. A* 331, 3-13.
- 854 Roy-Barman, M., Chen, J.H. and Wasserburg, G.J. (1996)  $^{230}\text{Th}$ - $^{232}\text{Th}$  systematics in the central Pacific  
855 Ocean: The sources and the fates of thorium. *Earth Planet. Sci. Lett.* 139, 351-363.
- 856 Roy-Barman, M., Coppola, L. and Souhaut, M. (2002) Thorium isotopes in the western Mediterranean  
857 Sea: an insight into the marine particle dynamics. *Earth Planet. Sci. Lett.* 196, 161-174.
- 858 Roy-Barman, M., Lemaître, C., Ayrault, S., Jeandel, C., Souhaut, M. and Miquel, J.C. (2009) The  
859 influence of particle composition on thorium scavenging in the Mediterranean Sea. *Earth Planet. Sci. Lett.*  
860 286, 526-534.
- 861 Rubin, M., Berman-Frank, I. and Shaked, Y. (2011) Dust- and mineral-iron utilization by the marine  
862 dinitrogen-fixer *Trichodesmium*. *Nature Geosci.* 4, 529-534.
- 863 Rue, E.L. and Bruland, K.W. (1995) Complexation of iron(III) by natural organic ligands in the Central  
864 North Pacific as determined by a new competitive ligand equilibration/adsorptive cathodic stripping  
865 voltammetric method. *Mar. Chem.* 50, 117-138.

- 866 Santschi, P.H., Murray, J.W., Baskaran, M., Benitez-Nelson, C.R., Guo, L.D., Hung, C.C., Lamborg, C.,  
867 Moran, S.B., Passow, U. and Roy-Barman, M. (2006) Thorium speciation in seawater. *Mar. Chem.* 100,  
868 250-268.
- 869 Schlosser, C. and Croot, P. (2008) Application of cross-flow filtration for determining the solubility of  
870 iron species in open ocean seawater. *Limnol. Oceanogr. Methods* 6, 630-642.
- 871 Serno, S., Winckler, G., Anderson, R.F., Hayes, C.T., McGee, D., Machalett, B., Ren, H., Straub, S.M.,  
872 Gersonde, R. and Haug, G.H. (2014) Eolian dust input to the Subarctic North Pacific. *Earth Planet. Sci.*  
873 *Lett.* 387, 252-263.
- 874 Tagliabue, A., Aumont, O. and Bopp, L. (2014) The impact of different external sources of iron on the  
875 global carbon cycle. *Geophys. Res. Lett.* 41, 2013GL059059.
- 876 Taylor, S.R. and McLennan, S.M. (1995) The geochemical evolution of the continental crust. *Rev.*  
877 *Geophys.* 33, 241-265.
- 878 Upadhyay, N., Majestic, B.J., Prapaipong, P. and Herckes, P. (2009) Evaluation of polyurethane foam,  
879 polypropylene, quartz fiber, and cellulose substrates for multi-element analysis of atmospheric particulate  
880 matter by ICP-MS. *Anal. Bioanal. Chem.* 394, 255-266.
- 881 Ussher, S.J., Achterberg, E.P., Powell, C., Baker, A.R., Jickells, T.D., Torres, R. and Worsfold, P.J.  
882 (2013) Impact of atmospheric deposition on the contrasting iron biogeochemistry of the North and South  
883 Atlantic Ocean. *Global Biogeochem. Cycles* 27, 1096-1107.
- 884 Ward, B.A., Dutkiewicz, S., Moore, C.M. and Follows, M.J. (2013) Iron, phosphorus, and nitrogen  
885 supply ratios define the biogeography of nitrogen fixation. *Limnol. Oceanogr.* 58, 2059-2075.  
886  
887

Figure 1

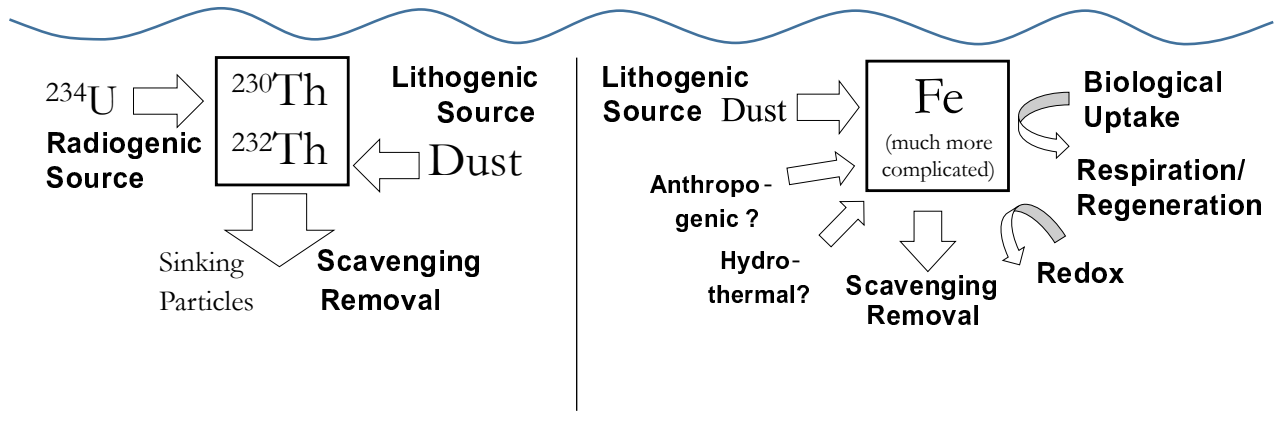


Figure 2

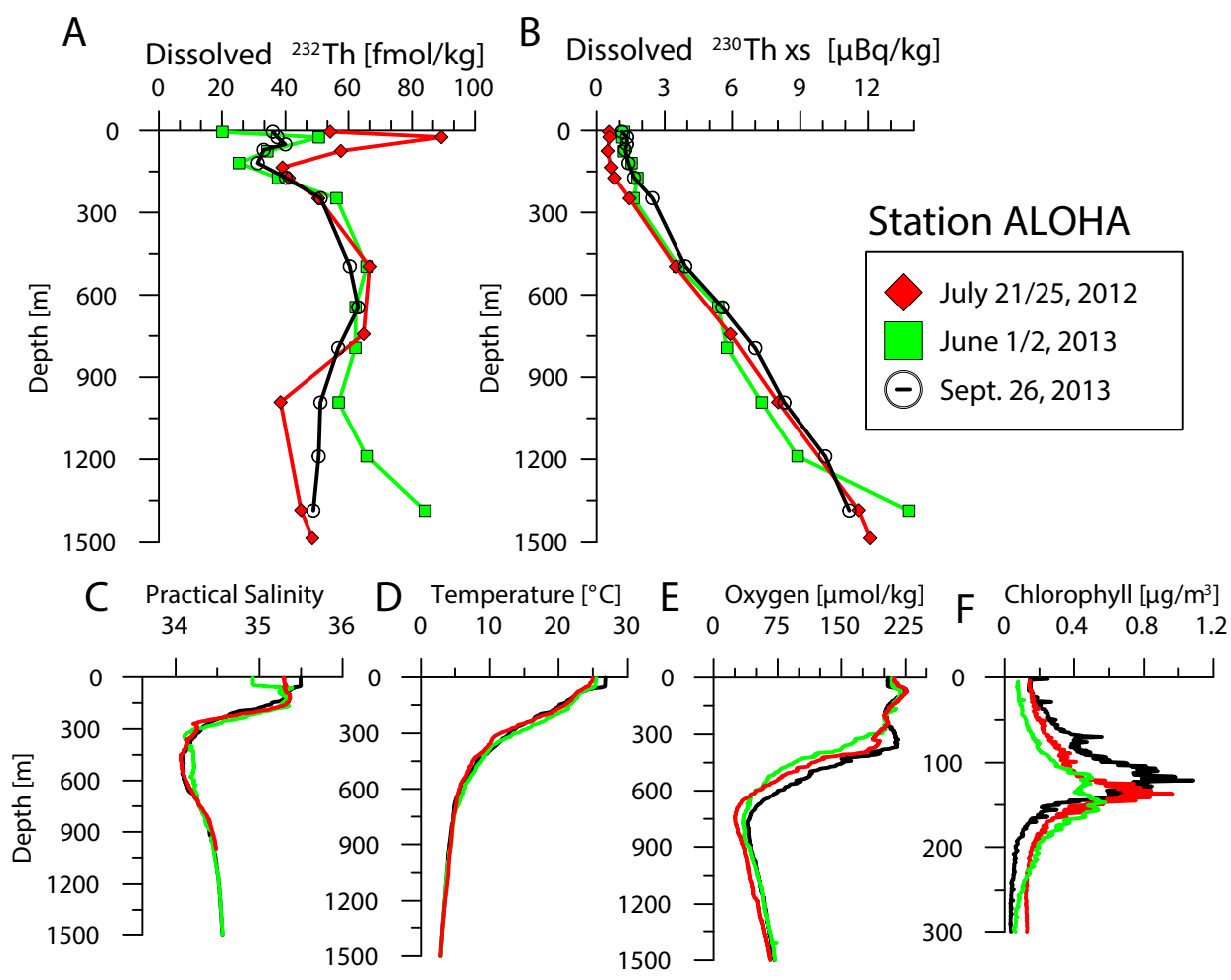
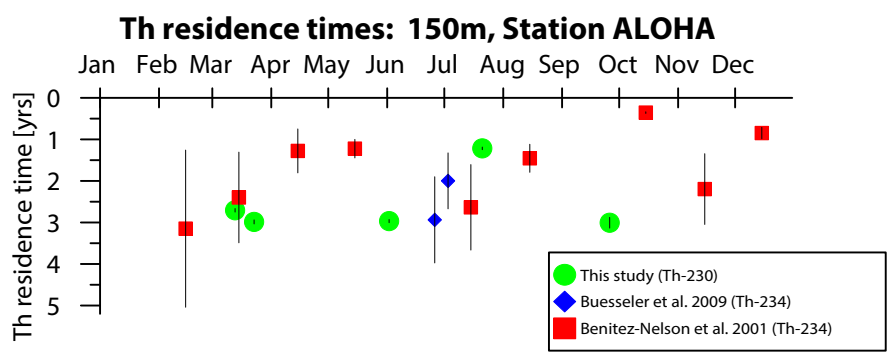
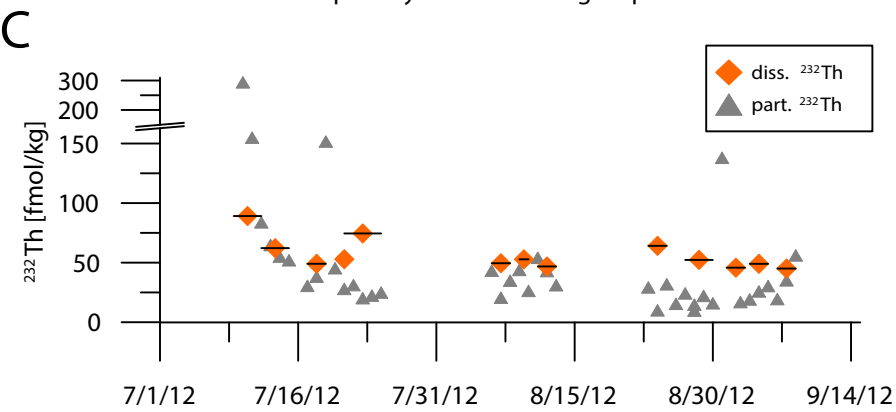
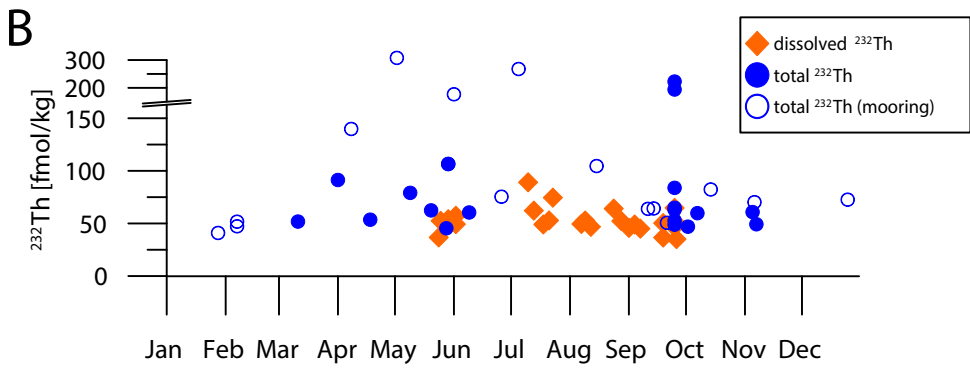
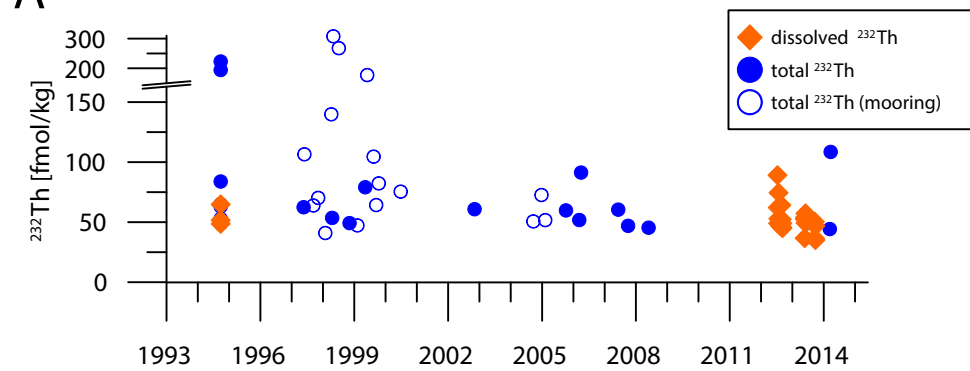
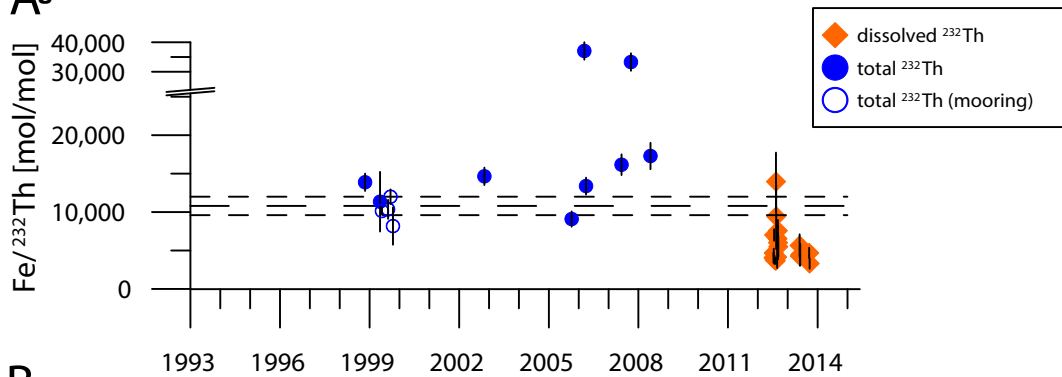
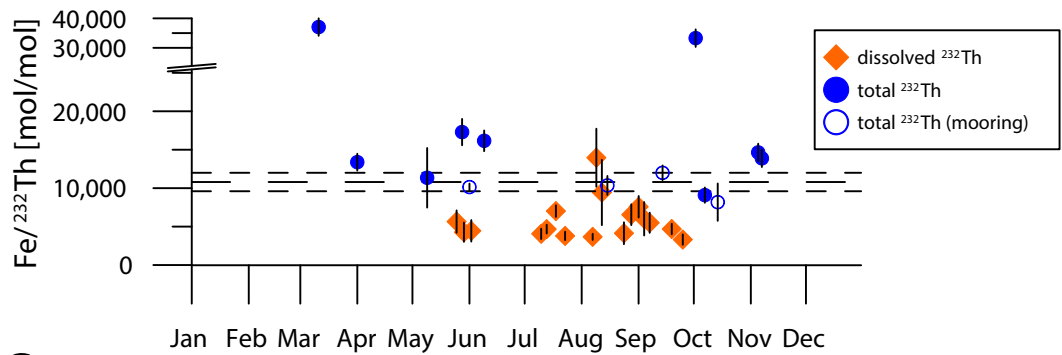
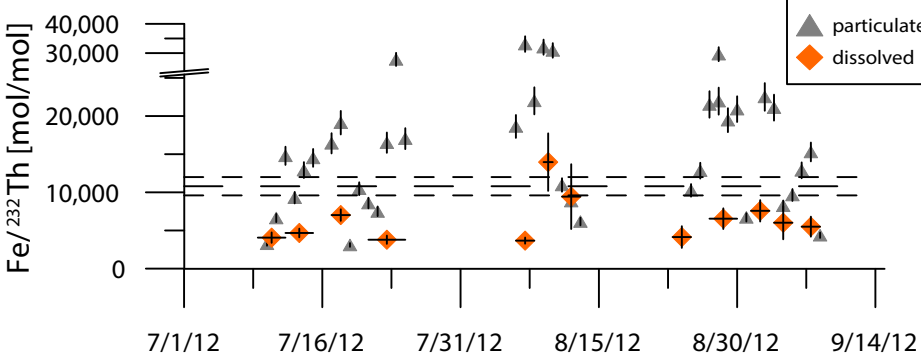


Figure 3



**Figure 4**

**Figure 5****B****C**

**Figure 6** % Colloidal metals (of dissolved)

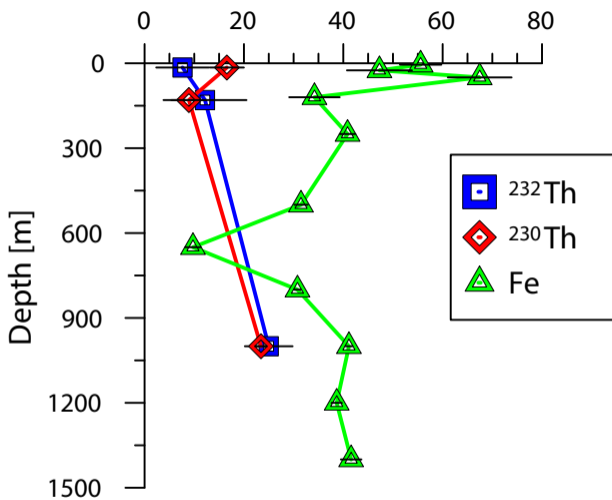




Figure 7

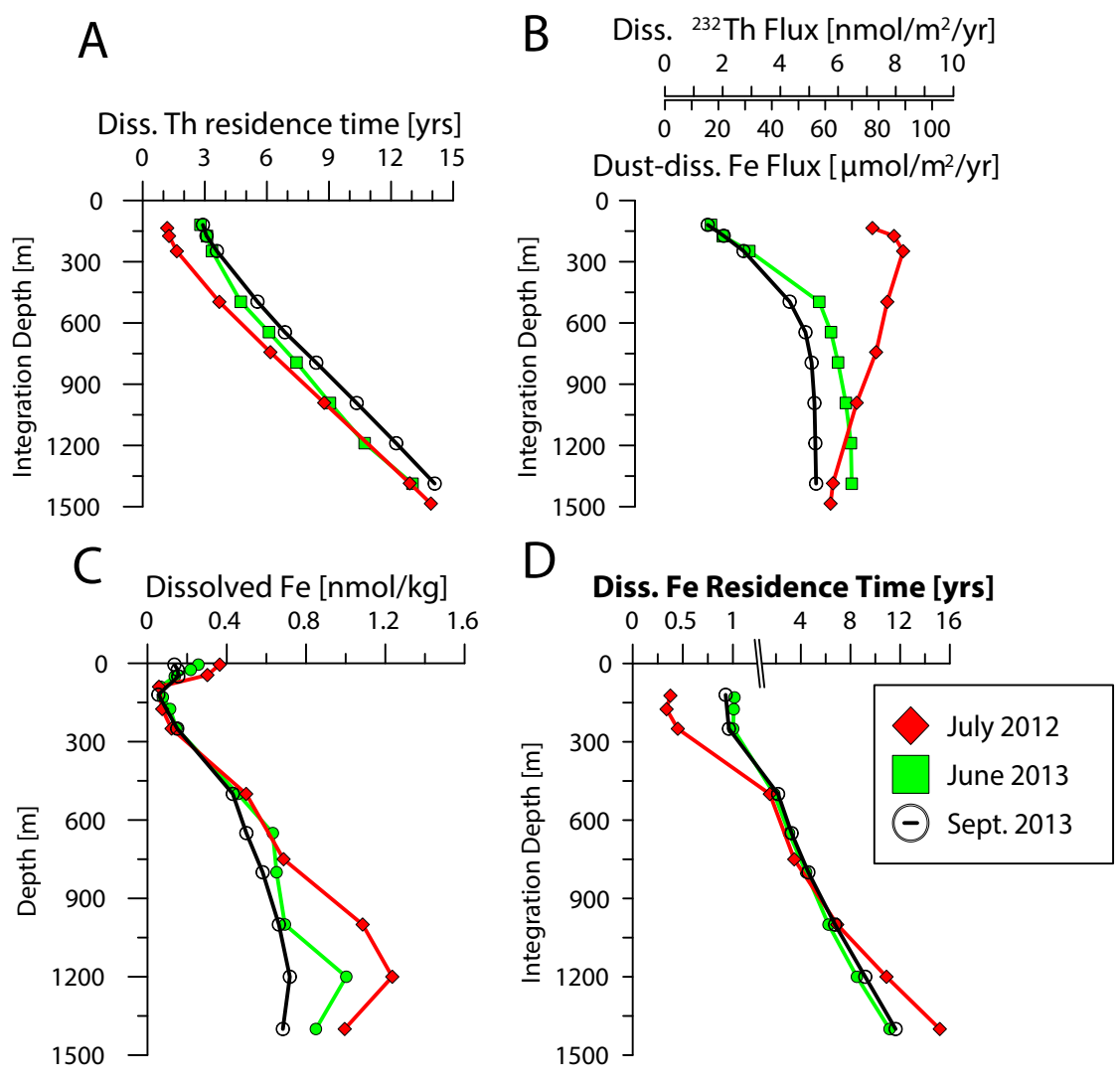


Figure 8

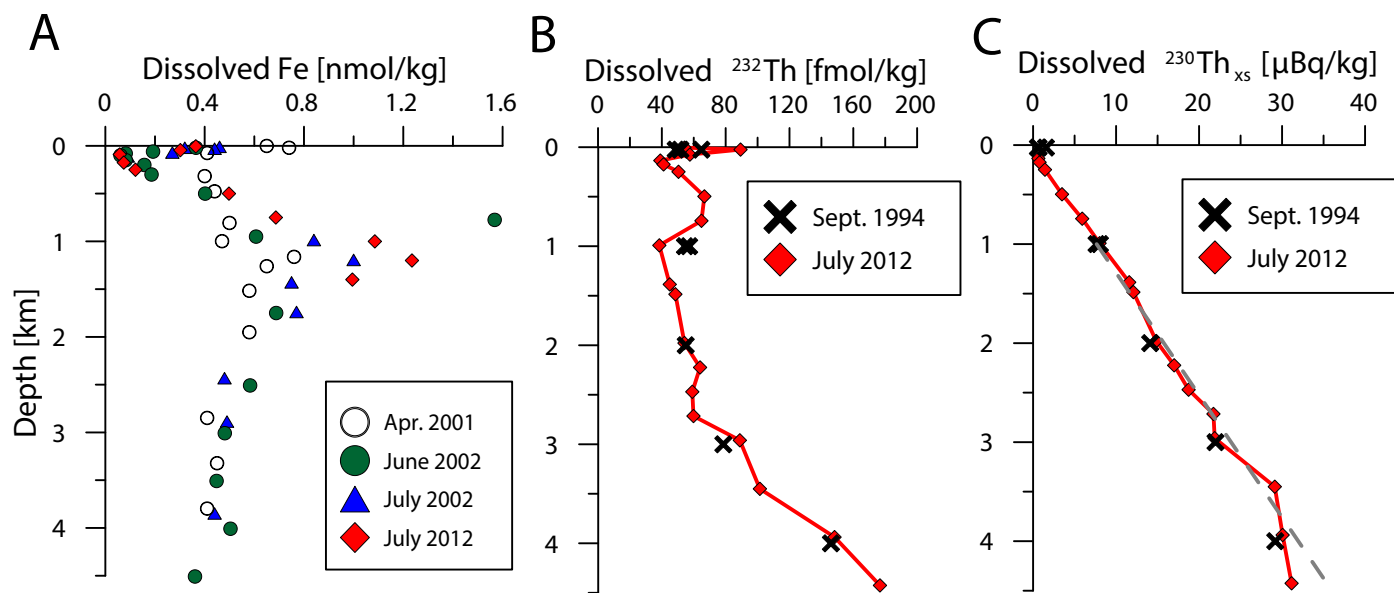
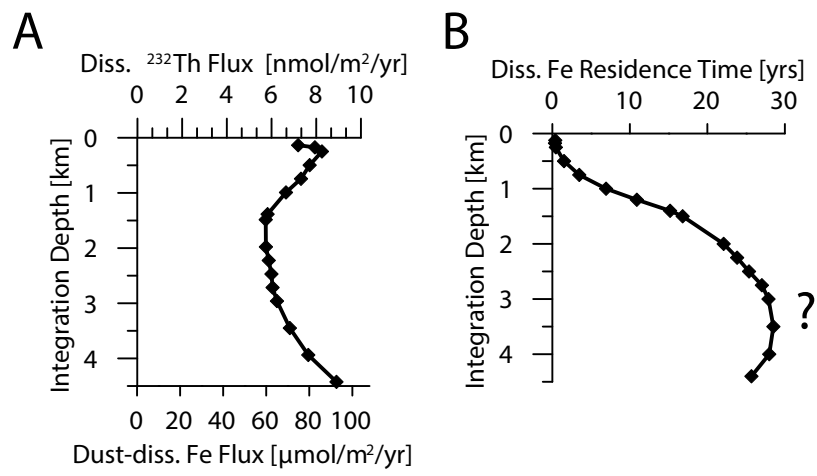


Figure 9



**Supplemental Data**

[Click here to download Electronic Annex: Hayes ALOHA Th Fe Supplemental Data for GCA.xlsx](#)